Pesticide Biochemistry and Physiology 221 (2026) 107143



Contents lists available at ScienceDirect

Pesticide Biochemistry and Physiology

journal homepage: www.elsevier.com/locate/pest

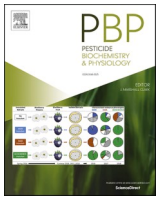

Network-pharmacology-guided elucidation of *Cornus officinalis*-mediated protection against paraquat-induced neurotoxicity via restoration of dopaminergic and GABAergic signaling pathways

Anas Yusuf [a], Murtala Bindawa Isah [a,b], Wenting Li [a], Xiaozhou Yang [a], Chen Chen [a], Alberto C.P. Dias [a,c,*], Xiaoying Zhang [a,c,*]

[a] Chinese-German Joint Institute for Natural Product Research, Shaanxi International Cooperation Demonstration Base, Shaanxi University of Technology, Hanzhong 723000, Shaanxi, China
[b] Department of Biochemistry, Umaru Musa Yar'adua University, Katsina, Nigeria
[c] Centre of Molecular and Environmental Biology (CBMA), Department of Biology, University of Minho, Campus de Gualtar, Braga 4710-057, Portugal

ARTICLE INFO

Keywords:
Cornus officinalis
Zebrafish model
Paraquat
Oxidative stress
Apoptosis
Dopaminergic signaling
GABAergic signaling
Synapse

ABSTRACT

Paraquat (PQ; 1,1′-dimethyl-4,4′-bipyridinium dichloride) is a widely used herbicide and environmental contaminant that disrupts neuronal homeostasis through oxidative stress and apoptosis, leading to dopaminergic and GABAergic dysfunction resulting in neurotransmitter imbalance and Parkinson's disease-like phenotype. Here, we combined phytochemical profiling, network pharmacology, molecular docking, and zebrafish-based assays to elucidate the neuroprotective mechanisms of *Cornus officinalis* ethanolic extract (COE). UHPLC–MS and HPLC–DAD analyses identified morroniside (133.50 mg/g dry extract) and loganin (62.90 mg/g dry extract) as the predominant constituents of COE. Integrative bioinformatics and transcriptomic analysis identified eight hub genes (*th*, *slc6a3*, *hspa8*, *syn2*, *gap43*, *gad1*, *sncb*, and *drd2*) as core targets of COE, with significant enrichment in dopaminergic and GABAergic synaptic pathways. Molecular docking further predicted a high binding affinity (-10.4 kcal mol^{-1}) between p-hydroxycinnamic acid and tyrosine hydroxylase. In vivo experiments demonstrated that PQ exposure (100 μM) induced reactive oxygen species (ROS) accumulation, apoptosis, and the transcriptional downregulation of neuro-markers in zebrafish larvae, resulting in measurable locomotor deficits. Conversely, COE co-treatment (5–20 μg/mL) attenuated ROS production and apoptotic cell death. These effects were accompanied by the upregulation of *nrf2* and *bcl-2*, and the restoration of *th* and *slc6a3* expression. Imaging of Tg(HuC:GFP) and Tg(Hb9:GFP) transgenic lines confirmed that COE preserves neuronal integrity, while behavioral assays validated the recovery of locomotor activity and light/dark responsiveness. Collectively, these findings demonstrate that COE exerts neuroprotection by modulating oxidative stress, inhibiting apoptosis, and stabilizing dopaminergic/GABAergic neurotransmission. This study positions *C. officinalis* as a potent therapeutic candidate for mitigating pesticide-induced neurodegeneration and provides a comprehensive mechanistic framework for its network-level actions.

1. Introduction

Environmental contaminants, including biological agents and synthetic agrochemicals, are increasingly recognized as significant contributors to the etiology of neurodegenerative diseases (NDs) (Flores-Gutierrez et al., 2023). A growing body of epidemiological and experimental evidence indicates a strong association between chronic pesticide exposure and an elevated risk of developing Parkinson's disease (PD) and other NDs (Baltazar et al., 2014). Among these agrochemicals, paraquat (PQ; 1,1′-dimethyl-4,4′-bipyridinium dichloride), a non-selective herbicide extensively applied in agriculture, has been repeatedly implicated as a major environmental risk factor for PD (Sharma and Mittal, 2024). Mechanistically, PQ exerts its neurotoxic effects through multiple converging pathways, including the induction

* Corresponding authors at: Chinese-German Joint Institute for Natural Product Research, Shaanxi International Cooperation Demonstration Base, Shaanxi University of Technology, Hanzhong 723000, Shaanxi, China.
E-mail addresses: isah.murtala@umyu.edu.ng (M.B. Isah), yangxiaozhou@snut.edu.cn (X. Yang), cchen@snut.edu.cn (C. Chen), albertocpdias66@gmail.com (A.C.P. Dias), zhang@bio.uminho.pt (X. Zhang).

https://doi.org/10.1016/j.pestbp.2026.107143
Received 22 October 2025; Received in revised form 25 April 2026; Accepted 25 April 2026
Available online 30 April 2026
0048-3575/© 2026 Elsevier Inc. All rights are reserved, including those for text and data mining, AI training, and similar technologies.

of oxidative stress (Alizadeh et al., 2022), activation of apoptotic cascades (Chung See et al., 2024), and stimulation of inflammatory signaling (Ghasemi et al., 2023), ultimately leading to progressive neuronal degeneration (Zhang et al., 2016). Notably, PQ can traverse the blood–brain barrier and directly target dopaminergic neurons within the nigrostriatal pathway (Darweesh et al., 2024; Liu et al., 2024; Sharma and Mittal, 2024). Once absorbed, PQ is metabolized into its monovalent cation (PQ^+), which acts as a substrate for the dopamine transporter (DAT). This facilitates its selective accumulation in dopaminergic neurons, where PQ^+ undergoes continuous redox cycling, producing superoxide and other reactive oxygen species. The resulting oxidative damage ultimately leads to neuronal injury and degeneration (Rappold et al., 2011). This selective vulnerability results in the disruption of neurotransmission, with marked dysregulation of dopaminergic and GABAergic pathways emerging as key mechanistic drivers of brain functional decline (Błaszczyk, 2016; Davis et al., 2023a). Alterations in these neurotransmitter systems are strongly correlated with the motor, cognitive, and behavioral deficits that characterize several major neurodegenerative disorders, including PD (Mironova et al., 2018; Zhang et al., 2019), and Alzheimer's disease (AD) (Bukke et al., 2020; Madeira et al., 2018). Gamma-aminobutyric acid (GABA), the principal inhibitory neurotransmitter in the central nervous system, plays a critical role in maintaining the excitation–inhibition (E/I) balance required for normal neural circuit function. Dysregulation of GABAergic signaling has been implicated not only in neurodevelopmental disorders but also in the progression of neurodegenerative pathologies (Błaszczyk, 2016; Ramamoorthi and Lin, 2011). The consistent findings from both human studies and animal models indicate the significance of PQ as an environmental contaminant that can contribute to the development of neurodegenerative pathology, highlighting an urgent need for therapeutic intervention.

Cornus officinalis Sieb. et Zucc. *(C. officinalis),* a traditional Chinese medicinal plant, has demonstrated neuroprotective and neurotrophic properties in various experimental models (Guo et al., 2025; Tian et al., 2019). This therapeutic potential of *C. officinalis* is attributed to its rich composition of bioactive compounds, including ursolic acid, morroniside, and various quercetin derivatives (Yang et al., 2023). Notably, ursolic acid and oleanolic acid, pentacyclic triterpenoids, exhibit neuroprotective effects and are known to influence neurotransmission and neurodevelopment (Chen et al., 2023), while morroniside, an iridoid glycoside, has shown significant neuroprotective capabilities by inhibiting oxidative stress and ferroptosis, preventing neuronal apoptosis, and supporting mitochondrial function (Li et al., 2023). These compounds collectively influence synaptic function, promote neuronal growth, and activate key signaling cascades relevant to neuronal survival and plasticity pathways, thereby contributing to neuronal regeneration and repair (Guo et al., 2024; Sánchez-Alegría et al., 2018). While *C. officinalis* and its metabolites show a promising pharmacological profile in diverse neurological contexts, its specific impact on PQ-induced neurotransmitter dysregulation, neurodevelopmental impairment, and related behavioral deficits remains largely to be investigated.

Zebrafish have emerged as a valuable model for investigating the toxicological effects of environmental contaminants and neurotoxins, due to its higher genetic homology with humans and the ability to monitor pathological progression in vivo (Jiang et al., 2025). Their body transparency during early development allows real-time visualization of neuronal growth and degeneration, while their permeability to water-soluble compounds makes them particularly well suited for high-throughput drug screening (Cassar et al., 2020). Leveraging these advantages, this study aimed to systematically evaluate the neuroprotective potential of ethanolic extract of *C. officinalis* in PQ-exposed wild-type and transgenic zebrafish models. Specifically, we investigated its ability to restore dopaminergic and GABAergic signaling, promote neuronal development, and ameliorate behavioral impairments. By integrating functional and behavioral assays with fluorescent imaging and gene expression profiling, this work seeks to establish *C. officinalis* as a candidate therapeutic agent for mitigating PQ-induced neurotoxicity and advancing strategies for neuroprotection and regeneration.

2. Materials and methods

2.1. Chemicals

All chemical standards used in this study were of HPLC grade with a purity of ≥98%, unless otherwise specified. Chlorogenic acid (Energy Chemicals); ursolic acid, oleanolic acid, loganin, gallic acid, morroniside, cornuside, rutin, and quercetin were from Shanghai Yuanye Bio-Technology Co., Ltd., China. UHPLC-UV grade acetonitrile (Fisher Chemicals), phosphoric acid (85%; DmReagents), and PQ (Shanghai Aladdin Bio-Chem Technology Co., Ltd., China).

2.2. Preparation of C. officinalis ethanolic extract

The berries of *C. officinalis* were obtained from Foping county (33.52°N, 107.99°E) located in the southern part of Shaanxi province (China). Before processing, the berries were identified by Professor Chen Chen of Shaanxi International Cooperation and Demonstration Base for Science and Technology, Shaanxi University of Technology, Hanzhong, China.

The fresh berries were thoroughly washed and sorted to remove all pedicels. They were subsequently flash-frozen at −80 °C for 48 h and then lyophilized using LGJ-18C freeze dryer (Foring Technology Development, Beijing, China). The resulting dried berries were pulverized into a fine powder with an ultra-high-speed grinding machine (Tianjin Tire Instruments Co., Ltd). The powdered biomass was stored in dark, in a desiccator containing freshly prepared silica to preserve its dryness until further analysis.

The ethanolic extract of *C. officinalis* (COE) was prepared using a modified method based on previous work by Fan et al. (2022). Briefly, 100 g of the powdered *C. officinalis* biomass was subjected to three sequential extractions with 1 L of 90% ethanol. Each extraction cycle was performed for 40 min at 40 °C with an ultrasonic power of 80 W. The combined filtrates were concentrated using a rotary evaporator (RV10, IKA, Baden-Württemberg, Germany) at 50 °C. The concentrated extract was then lyophilized to a powder and stored at −20 °C in the dark for subsequent analysis and experiments.

2.3. Characterization and quantification of COE constituents by UHPLC–MS and HPLC-DAD

The comprehensive chemical composition of the COE was characterized using Ultra-High Performance Liquid Chromatography coupled with a Q-Orbitrap Mass Spectrometer (UHPLC–Q-Orbitrap-MS). Chromatographic separation was achieved on a Waters HSS T3 column (100 × 2.1 mm, 1.8 μm) maintained at 40 °C. The mobile phases consisted of Milli-Q water with 0.1% formic acid (Phase A) and acetonitrile with 0.1% formic acid (Phase B). A flow rate of 0.3 mL/min was employed under the following gradient program: 0–1 min, 100% A; 1–12 min, linear increase to 95% B; 12–13 min, held at 95% B; 13.1–17 min, re-equilibration to 100% A. Sample injection volume of 2 μL was used. High-resolution mass spectrometry (HRMS) data were collected in both positive and negative ion modes using a heated electrospray ionization (HESI) source. The HESI source was operated with a sheath gas flow of 40 arbitrary units (arb) and an auxiliary gas flow of 10 arb. The spray voltage was set at +3000 V for positive mode and − 2800 V for negative mode. The capillary and ion transfer tube temperatures were 350 °C and 320 °C, respectively. The mass scan range for the MS2 was m/z 70–1050. The mass resolving power was set at 70,000 for MS1 and 17,500 for MS^2.

For quantification, COE samples and reference standards were analyzed using a Thermo UltiMate 3000 UPLC system (Thermo Fisher

Scientific, Waltham, MA, USA) equipped with a quaternary pump, autosampler, column thermostat, sample tray, and diode array detector (DAD). Chromatographic separation was carried out on an Inertsil ODS-3 column (4.6 × 250 mm, 4 μm; GL Sciences, Tokyo, Japan). The mobile phases were (A) water containing 0.1% (*v*/v) phosphoric acid and (B) acetonitrile, with the following gradient program: 0–1 min, 95% A; 1–2 min, 90% A; 2–25 min, 55% A; 25–30 min, 5% A; 30–45 min, 5% A; 45–50 min, 95% A. The flow rate was 1.0 mL/min, column temperature was maintained at 30 °C, detection was monitored across 210–500 nm, and the injection volume was 20 μL. Quantification was performed from the standard curves obtained from pure compounds. Gallic acid, morroniside, loganin, sweroside, cornuside, oleanolic acid, and ursolic acid were quantified directly using standard compounds. Cinnamic acids, galloylquinic acid, and quercetin derivatives were quantified as chlorogenic acid, gallic acid, and rutin equivalents, respectively.

2.4. Target identification

SMILES of all the compounds where obtain from Pubchem (https://pubchem.ncbi.nlm.nih.gov/). To identify the target proteins of both PQ and COE metabolites, two databases were used: the Comparative Toxicogenomics Database (CTD), an open-source resource predicting chemical-gene interactions (Davis et al., 2023b), and SwissTarget Prediction server (https://www.swisstargetprediction.ch/) which is a web-based database for predicting potential target genes using SMILES. For more relevance, large dataset from Gene Expression Omnibus (GEO, https://www.ncbi.nlm.nih.gov/geo/query/acc.cgi?acc=GSE182622) with accession ID of GSE182622 (Tiklová et al., 2021) consisting 86 normal control samples and 106 PD patient samples mRNA expression profiles of dopaminergic neurons in both PD and normal control subjects were selected for analysis. Data analysis was carried out using GEO2R function on the NCBI site. For differential gene expression analysis, adjusted p-value < 0.05 were set as statistical significance. Additionally, high throughput single-cell sequencing dataset (GSE178265 (SCP1768)) from midbrain dopamine neurons in the substantia nigra pars compacta were also utilized for comparison (Kamath et al., 2022). All single-cell data analysis was carried out in Single Cell Portal (https://singlecell.broadinstitute.org/single_cell). Results from these datasets are then analyzed through Venn diagram to identify overlapping genes.

2.4.1. Network construction, identification of hub genes, functional annotation, and pathway enrichment analysis

A network containing COE metabolites and there corresponding target genes, and protein interaction of common targets from PQ and COE were constructed using cytoscape (Otasek et al., 2019). Furthermore, Hub genes were identified from merging all the common target genes in the datasets and common genes from PQ and COE targets, the analysis was carried out using cytoHubba (Chin et al., 2014) plugin utilizing three algorithms, including Edge Percolated Component (EPC), Maximal Clique Centrality (MCC), and degree. From each algorism, top ten genes were identified, finally, the intersected genes from this analysis are considered to be the hub genes. All functional annotations and pathway enrichment analysis in this work was performed using DAVID Bioinformatics, a web server tool from NCBI (https://davidbioinformatics.nih.gov/home.jsp).

2.4.2. miRNA-hub gene network construction, co-expression and functional analysis

With the aim to explore whether the hub genes might have similar or common regulatory miRNAs which are known to regulate post-transcriptional gene expression either via inhibiting mRNA translation or promoting mRNA degradation (Correia de Sousa et al., 2019). An important web-based server called miRDB database (https://mirdb.org) was used to predict potential miRNA that might regulate each hub gene and the corresponding miRNA-Hub gene networks was constructed using cytoscape. To facilitate the co-expression analysis of the selected hub genes, we employed the GeneMANIA web resource (https://genemania.org/) (Franz et al., 2018), This robust bioinformatics platform was leveraged due to its capacity to construct predictive gene interaction networks through the integration of multiple distinct data sources, including shared protein domains, physical/genetic interactions, and co-localization patterns. The resulting network was thus tailored to visualize and hypothesize relationships specifically among the identified drug target genes.

2.5. Molecular docking

All receptor proteins, except HSPA8 and SYN2, were obtained from UniProt (https://www.uniprot.org/), these two receptors were model using SWISS-MODEL (http://swissmodel.expasy.org) a server for automated comparative structural modeling of three-dimensional (3D) protein structures. All ligands (COE metabolites) 3D structures were obtained from PubChem (https://pubchem.ncbi.nlm.nih.gov/) in SDF format which later converted to Protein Data Bank, Partial Charge (Q), and Atom Type (T) (PDBQT) using open OpenBabel software (O'Boyle et al., 2011). All molecular docking was performed in AutoDock Vina (Trott and Olson, 2010). to calculate binding energies, and Visualizations of docking results were performed with Discovery studio.

2.6. Zebrafish maintenance and embryo collection

Adult wild-type and transgenic Zebrafish were obtained from National Aquatic Germplasm Bank, Institute of Hydrobiology, Chinese Academy of Sciences. zebrafish were housed in a recirculating water system (LY-BMY50 Lingyun Boqi Technology Co., Ltd., Beijing, China), and maintained under stable conditions; a temperature of 28 ± 0.5 °C, a 14/10-h light/dark cycle, and twice-daily feeding with flake food. Eggs were collected from natural spawning events and washed in E3 medium (NaCl 5 mM, KCl 0.17 mM, $CaCl_2$ 0.33 mM, and $MgSO_4$ 0.33 mM; pH 7.4). Fertilized eggs were kept in E3 medium, and incubated at 28 ± 0.5 °C (Silva et al., 2021).

2.7. Zebrafish embryotoxicity and COE dose-response assessment

Previous study reported mitochondrial dysfunction in zebrafish larvae exposed to 100 μM PQ without causing mortality or gross deformities (Wang et al., 2018). Based on this, at 3–4 h post-fertilization (hpf) zebrafish embryos were exposed to a varying concentration of PQ (25, 50, and 100 μM) prepared in E3 medium ($n = 20$ per replicate). The medium was refreshed every 24 h until the larvae reached 4 days post-fertilization (dpf).

To evaluate the toxicity of the COE, 3 dpf larvae were exposed to COE at concentrations ranging from 0 to 500 μg/mL prepared in E3 medium (n = 20 per replicate). Larvae were washed and the medium was replaced every 24 h. Throughout the experiment; mortality was recorded daily until 6 dpf. All experimental procedures were approved by the Institutional Review Board of the Chinese-German Joint Institute for Natural Product Research, Shaanxi University of Technology (2025-05).

2.8. Morphological examination for malformation, hatchability, and heartbeat

Morphological observation of embryos was carried out on a stereo microscope at 24-h intervals (ZOOM-7045, Shanghai Shanqian Optical Instrument Co., Ltd., China). Embryos exposed to PQ or COE, as well as control groups were monitored from 3 to 4 hpf to 4 dpf. Developmental parameters, including hatchability, mortality, malformation, and heartbeat rate were evaluated. Hatching rate was assess by counting the number of embryos emerging from the chorion. Body length, as well as the areas of the cardiac region and yolk sac, were measured with ImageJ (NIH, National Institutes of Health, Bethesda, MD, USA). Heartbeats were counted manually for one minute under the microscope and are

presented as the mean beats per 30 s (Thilini et al., 2024).

2.9. In vivo antioxidant activity assay

The levels of reactive oxygen species (ROS) were quantified in whole-body zebrafish larvae at 96 hpf. Larvae were treated with either E3 only, PQ only (100 μM), or co-incubated with COE at concentrations of 5, 10, or 20 μg/mL, or treated with COE alone at 20 μg/mL. ROS levels were measured using chloromethyl-2′,7′-dihydrodichlorofluorescein diacetate (CM-H_2DCFDA; Molecular probes). The larvae in all groups were washed three times using E3 medium and then the probe was added to a final concentration of 10 μM and incubated in the dark for 40 min at 28 °C. Subsequently, the excess probe was removed by washing 3 times with E3 medium, and larvae anesthetized with 50 mg/L benzocaine, and positioned laterally on glass slide for imaging. The level of ROS was examined using a fluorescent microscope (M205FCA/K3C, Leica, Wetzlar, Hessian, Germany). The fluorescent intensities of the larval images were quantified using ImageJ (National Institutes of Health, Bethesda, Maryland, USA) (Bashirova et al., 2023).

2.10. Apoptosis assay

The level of apoptosis in the whole body of larvae was assess using acridine orange (AO) staining as described by (Saputra et al., 2024). A pool of ten larvae per replicate (thirty larvae per treatment) was exposed to either E3, PQ-only (100 μM) or co-incubated with COE at 5, 10, and 20 μg/mL or COE only at 20 μg/mL from 3 to 4 hpf to 96 hpf, the larvae were washed after every 24 h and new medium is replaced. At 96 hpf, the larvae were washed three times with E3 medium and OA (Sigma Aldrich) was added to final concentration of 5 μg/mL in E3 medium and incubated for 30 min in the dark at 28 °C. Embryos were washed three times with E3 medium. and anesthetized with 50 mg/L benzocaine and, positioned laterally on glass slide for imaging. Apoptosis was examined using a fluorescent microscope. The images of larvae with areas of apoptotic cells with fluorescent AO positivity were quantified using ImageJ software (National Institutes of Health, Bethesda, Maryland, USA) (Bashirova et al., 2023).

2.11. Fluorescence imaging of transgenic zebrafish and neuronal integrity assessment

Two transgenic zebrafish lines were utilized to evaluate the neuroprotective effects of the COE and to visualize specific neuronal populations, The Tg(HuC:GFP) line, which expresses enhanced green fluorescent protein (eGFP) under the control of the HuC (*elavl3*) promoter, was used for pan-neuronal labeling. This enabled the visualization of general neuronal populations, assessment of their morphology, and observation of overall nervous system development. The Tg(Hb9:GFP) line (also known as Tg(mnx1:GFP)), which specifically labels motoneurons, was used for a targeted analysis of motor neuron integrity.

At 6 dpf, larvae from all experimental groups were anesthetized with 50 mg/L benzocaine. They were then mounted in 1.0% low-melting-point agarose on glass slides for whole-body fluorescence imaging (M205FCA/K3C, Leica, Wetzlar, Hessian, Germany). The resulting images were analyzed using ImageJ. All imaging parameters were kept consistent across the experimental and control groups.

2.12. Behavioral analysis

Behavioral assessments were conducted to evaluate the neurological and sensorimotor responses of zebrafish larvae following treatment.

2.12.1. Free locomotive activity test

Wild-type zebrafish from all treatment and control groups at 8 dpf were individually placed in 24-well plate, each containing 500 μL of E3 medium. After an acclimatization period of 10 min under standard conditions, spontaneous locomotor activity was recorded for 30 min using the ZebraBox video tracking system (Viewpoint, Lyon, France). Parameters including total distance traveled, movement speed, and swim pattern trajectories were analyzed to assess general locomotor behavior.

2.12.2. Light/dark test

To evaluate sensorimotor responses, wild-type larvae from all experimental groups at 8 dpf were placed in a 24-well plate with 500 μL of E3 medium per well. After a 10 min acclimatization period, the larvae were subjected to alternating light and dark phases (5 min each) over a total duration of 30 min. Behavioral responses, including changes in activity levels and movement trajectories in response to light-dark transitions, were recorded using the ZebraBox video tracking system (Zhao et al., 2024).

2.13. RNA extraction, cDNA synthesis and real-time PCR

Total RNA was extracted from whole body of zebrafish larvae ($n = 30$ pooled per replicate, across three biological replicates) at 6 dpf across three independent biological replicates for each treatment and control groups. Larvae were rinsed three times with E3 medium, anesthetized using benzocaine, and snap-frozen in liquid nitrogen. RNA was isolated using TRIzol™ reagent (Invitrogen, Carlsbad, CA, USA), and the purity and concentration were assessed using a NanoDrop spectrophotometer (Thermo Fisher Scientific, Waltham, MA, USA). Complementary DNA (cDNA) was synthesized from total RNA using the FastKing cDNA Synthesis Kit (Tiangen Biotech, Beijing, China), following the manufacturer's instructions. Quantitative real-time PCR (RT-qPCR) was performed using the SuperReal PreMix Plus SYBR Green system (Tiangen Biotech, China) on a Bio-Rad CFX96 real-time PCR detection system (Bio-Rad Laboratories, Hercules, CA, USA).

The fold changes for relative mRNA expression of each gene were calculated using $2^{-\Delta\Delta C}_{T}$ method. Four housekeeping genes were tested, including *β-actin1* (*actb1*), Elongation factor 1 alpha (*ef1α*), 18 s, and Beta-2-microglobulin (*b2m*). The stability of all these genes across the treatment groups were validated using a Refinder (https://www.ciidirsinaloa.com.mx/RefFinder-master/) (Fig. S1). All the relative mRNA expressions were normalized using extended method of $2^{-\Delta\Delta C}_{T}$ method (Riedel et al., 2014). All primers and their sequences are listed in Table S1 (supplementary material).

2.14. Data and statistical analysis

All data analysis was performed using GraphPad Prism software version 9 (GraphPad Software, Boston, USA). One-way and two-way analyses of variance were used to determine significant differences (* $p < 0.05$, ** $p < 0.01$, and *** $p < 0.001$) between the mean values of all the experimental groups. All experimental data are expressed as mean ± standard deviation.

3. Result and discussion

3.1. Phytochemical analysis of COE

Untargeted UHPLC analysis performed in negative and positive electrospray ionization modes (Fig. S2) revealed a diverse profile of phytochemicals in COE, including iridoid glycosides, flavonoids, and phenolic acids, identified on the basis of their mass-to-charge ratios (Table S2). Structural confirmation was achieved through HPLC-DAD by comparing characteristic UV–Vis spectra and retention times with those of pure standards (Fig. S3). The major constituents identified include loganin, morroniside, ursolic acid, oleanolic acid, cornuside, and sweroside, well-recognized for their pharmacological activities and contribution to the therapeutic potential of *C. officinalis*. In addition, quercetin derivatives, caffeoylquinic acids, and gallic acid were also

detected and identified, all of which have been associated with antioxidant, neuroprotective, and anti-inflammatory properties (Gao et al., 2021). Among the compounds, the iridoid glycosides are the most prevalent, namely morroniside (133.3 mg/g DE) and loganin (62.9 mg/g) (Table 1).

3.2. Compounds-target network and enrichment analysis

Differentially expressed genes (DEGs) identified from GSE182622, which compared dopaminergic neurons from PD patients and healthy controls (Fig. 1A), were integrated with multiple target gene datasets. These included genes predicted to be targeted by COE metabolites (after data cleaning and duplicate removal), 18,129 genes retrieved from GeneCards using "Parkinson's disease" as the search query, and 672 genes associated with PQ exposure. In addition, DEGs from GSE178265 were incorporated into the analysis. The overlapping genes among these datasets were visualized using a Venn diagram to identify shared targets and potential intersections (Fig. 1B). Thirteen genes were identified to be common genes between all the datasets. Enrichment analysis of these genes reveals that dopaminergic and GABAergic synapses as the main pathways (Fig. 1C). For the purpose of this study, the common target genes were then merged with all the targets between PQ and COE metabolites after duplicates removal, a sum of 92 genes were identified and PPI network of these genes were constructed using Cytoscape (Fig. 1D). A representative network of COE metabolites with their corresponding target genes shows a complex interaction between these compounds and their potential regulatory genes (Fig. 1E). KEGG pathway enrichment analysis identified tyrosine metabolism, neuroactive ligand–receptor interaction, and the cAMP signaling pathway as the primary pathways associated with environmental information processing. Apoptosis and mitophagy are the main enriched pathways in cellular process while dopaminergic and GABAergic synapses are the most highly enriched pathways in relation to organismal systems (Fig. 1F), suggesting that COE metabolites potentially exert multifaceted neuroprotective effects against PQ by modulating neurotransmission and cellular survival networks.

3.3. Identification of hub genes and gene ontology (GO) analysis, and miRNA-hub genes analysis

To identify potential hub genes, we employed the CytoHubba plugin in Cytoscape, integrating three topological algorithms: Degree, EPC, and MCC. Genes that consistently ranked among the top ten across these algorithms were selected as hub genes (Fig. 1G–I). Through this systematic approach, eight hub genes were identified, including *syn2*, *sncb*, *gap43*, *gad1*, *hspa8*, *slc6a3*, *drd2*, and *th* (Fig. 1J). Due to the importance of these genes, we investigate their transcriptional profiles in midbrain dopaminergic neurons derived from patients with PD using single-nucleus RNA sequencing data. This analysis revealed a reduced expression of *syn2*, *sncb*, *gap43*, *gad1*, *hspa8*, and *th* in dopaminergic neurons. In contrast *slc6a3* and *drd2* exhibited moderate expression levels (Fig. 2A), which may reflect their differential regulatory dynamics in PD. GO enrichment analysis was performed to elucidate the functional roles of the gene set across three major categories: Biological Process (BP), Molecular Function (MF), and Cellular Component (CC). The BP category revealed significant enrichment in response to xenobiotic stimulus, chemical synaptic transmission, and negative regulation of apoptosis terms (Fig. 2B). The MF category showed enrichment in identical protein binding and ATP binding (Fig. 2C). In the CC category, the genes were predominantly associated with the cytoplasm, plasma membrane, and cytosol (Fig. 2D). These results highlight the central role of these genes in synaptic signaling, cellular stress responses, and apoptotic regulation.

To further investigate post-transcriptional regulatory mechanisms of the hub genes, miRNA–hub gene interactions were predicted using miRDB database. A total of 600 miRNAs with a target score ≥ 50 were identified. Among the hub genes, *syn2* exhibited the highest number of predicted regulatory miRNAs ($n = 177$), followed by *gad1* ($n = 91$), *gap43*($n = 87$), and *slc6a3* ($n = 82$). Additionally, *hspa8, sncb,* and *drd2* was predicted to be targeted by 68, 47, and 45 miRNAs, respectively. Whereas *th* was associated with only 9 predicted regulatory miRNAs. Notably, 16 miRNAs were predicted to target two or more among the hub genes (Fig. 2E), suggesting their potential role as key regulatory nodes within the PD-related molecular network.

3.4. Co-localization and molecular docking analysis

To gain deeper insights into the regulatory mechanisms of the identified hub genes, we employed the GeneMANIA webserver to construct a comprehensive gene–gene interaction network. Analysis of the interaction revealed that physical interactions accounted for 29.11%, co-expression contributed 24.60%, co-localization represented 3.55%, pathway-based interactions comprised 6.20%, and predicted interactions constituted the largest proportion at 36.53%. Functional analysis through GeneMANIA further demonstrated that these hub genes are significantly enriched in critical neurobiological processes, including dopamine uptake, monoamine transport, and neurotransmitter transport (Fig. 3A). These data further support the central role of the identified hub genes in neurotransmission and dopaminergic signaling, which are fundamental processes implicated in the pathophysiology of multiple neurodegenerative disorders.

Molecular docking was subsequently performed to validate the predicted regulatory interactions between the COE compounds and the identified hub genes. Binding energy is a key thermodynamic parameter indicative of the strength and stability of ligand–protein interactions, with lower values typically reflecting stronger binding affinity. The docking results were summarized and visualized as a binding energy heatmap (Fig. 3B), providing a comparative overview of compound–target interactions. Notably, most of the compounds exhibited high binding affinities toward tyrosine hydroxylase, with binding energies ranging from -5.5 kcal mol^{-1} for gallic acid to -10.4 kcal mol^{-1} for *p*-hydroxycinnamic acid. The interaction between *p*-hydroxycinnamic acid and TH involved five hydrogen bonds and one π-alkyl bond, with THR-426, GNL-425, GNL-428, ASP-424, SER-326, and PRO-323 identified as key interacting residues. Similarly, strong binding was observed with SLC6A3, with energies ranging from -4.4 kcal mol^{-1} for gallic acid to -9.6 kcal mol^{-1} for quercetin 3-O-β-D-glucuronide. These interactions involved three hydrogen bonds, one π-alkyl bond, and one

Table 1
Phytochemical composition of COE determined by UHPLC and HPLC-DAD.

Peak	Compound	RT	Formula	M/z	Mode	Amount (mg/g of DE)
1	5-galloylquinic acid	6.443	$C_{14}H_{16}O_{10}$	343.07	neg	10.40
2	Gallic acid	6.56	$C_7H_6O_5$	169.01	neg	5.50
3	Morroniside	9.947	$C_{17}H_{26}O_{11}$	405.14	neg	133.50
4	Loganin	11.75	$C_{17}H_{26}O_{10}$	449.17	neg	62.90
5	Sweroside	12.42	$C_{16}H_{22}O_9$	359.13	pos	33.10
6	p-Hydroxy-cinnamic acid	12.683	$C_9H_8O_3$	163.04	neg	19.0
7	Ferulic acid	15.113	$C_{10}H_{10}O_4$	193.05	neg	4.90
8	Quercetin 3-O-(6-O-malonyl)-b-D-glucoside	16.583	$C_{24}H_{22}O_{15}$	609.11	neg	6.80
9	Quercetin 3-O-Beta-D-Glucuronide	17.04	$C_{21}H_{18}O_{13}$	477.07	neg	10.50
10	Cornuside I	17.483	$C_{24}H_{30}O_{14}$	541.16	neg	37.90
11	Oleanolic acid	39.007	$C_{30}H_{48}O_3$	455.35	neg	4.70
12	Ursolic acid	38.678	$C_{30}H_{48}O_3$	455.35	neg	2.60

Amount = mg compound per g extract or per g dry extract, RT = Retention time, M/z = mass-to-charge ratio.

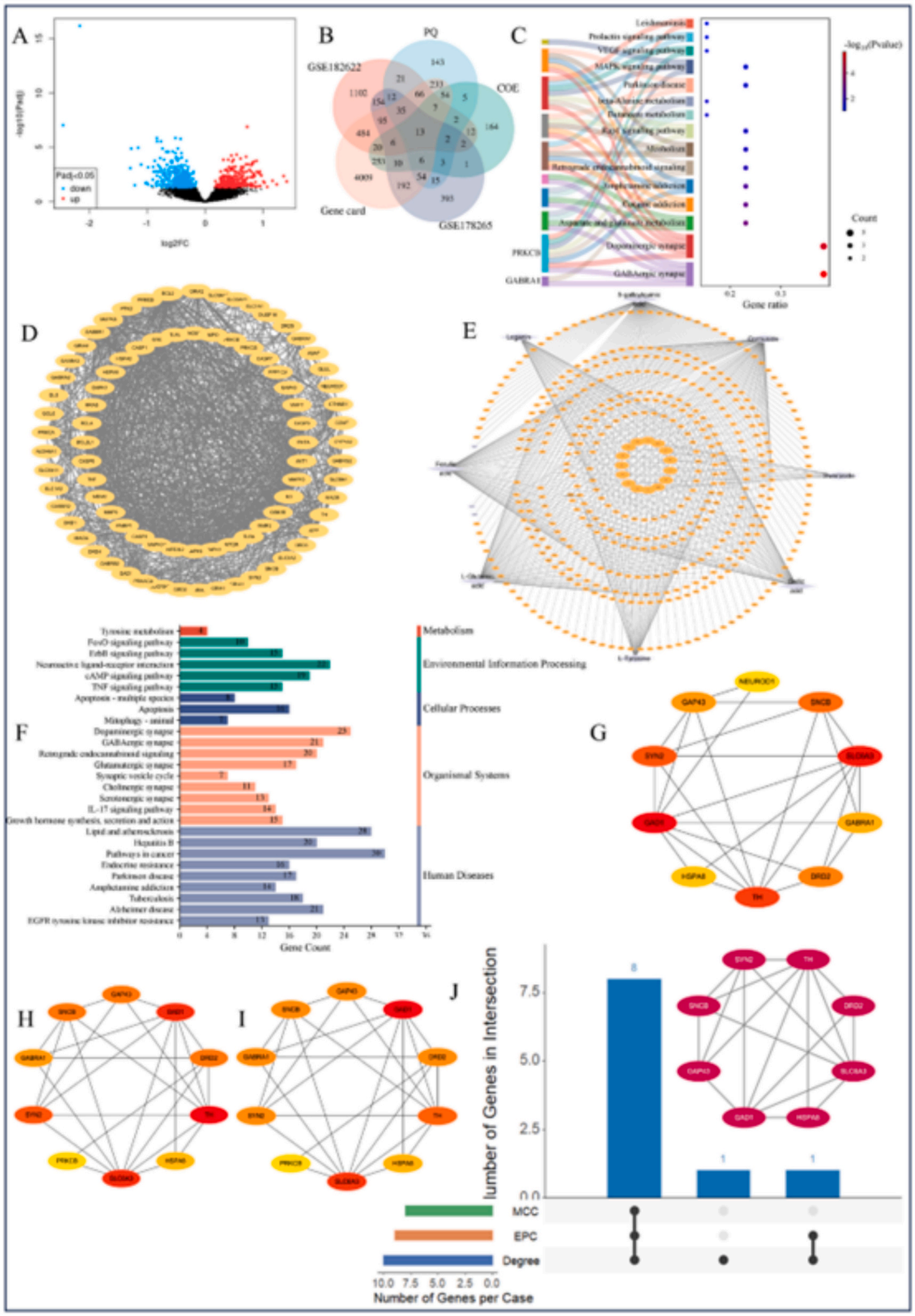

Fig. 1. Identification of potential molecular targets of COE compounds in PD. (A) Volcano plot showing differentially expressed genes (DEGs) between PD and normal controls. (B) Venn diagram integrating differentially expressed genes from bulkRNA-seq and single-cell nuclear sequencing, PD related gene set from GeneCards, PQ target genes from CTD database and COE compounds target genes. (C) Sankey plot showing enrichment of common genes. (D) Protein-protein interaction network of common COE and PQ targets. (E) Representative COE compounds and their target network interaction. (F) KEGG pathway summary of the target genes. (G-I) represent top ten hub genes identified using three algorithms of CytoHubba Degree, EPC, and MCC, respectively. (J) Upset plot demonstrating the intersection of hub genes across the three ranking algorithms.

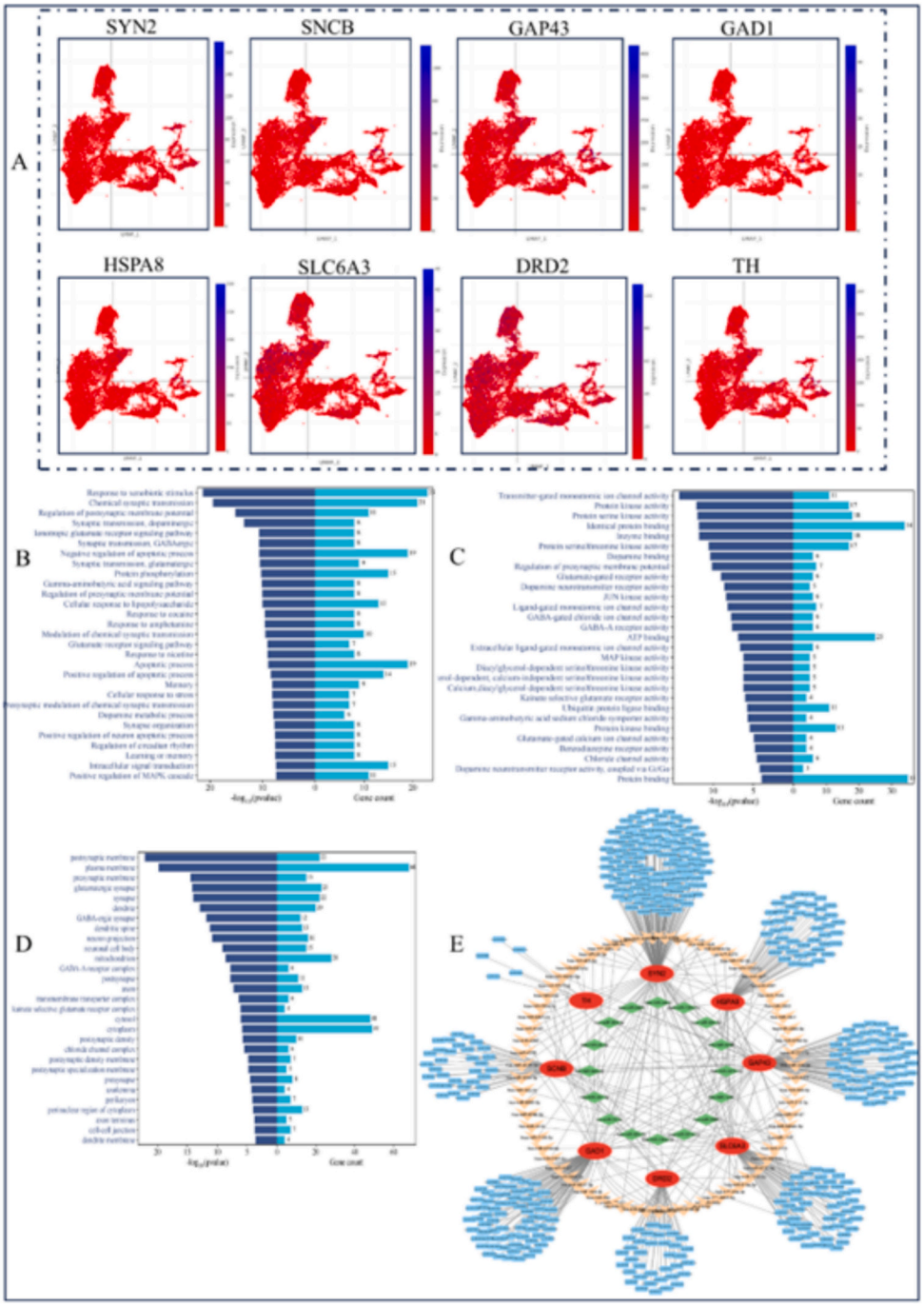

Fig. 2. Functional enrichment analysis and miRNA regulatory network analysis. (A) Expression profile of hub genes in dopaminergic neurons. (B-D) GO enrichment analysis of Biological Process (BP), Molecular Function (MF), and Cellular Component (CC), respectively. (E) miRNA regulatory network of hub genes.

π–π T-shaped interaction, with ASP-421, VAL-266, PHE-332, LYS-257, and SER-254 as the principal contributing residues (Fig. 3C). Collectively, these docking results provide evidence supporting the potential regulatory interactions between COE-derived bioactive compounds and key dopaminergic targets.

3.5. Embryotoxicity profiling and dose-response determination of PQ and COE in the zebrafish larvae

A three-point time-resolved dose-response acute toxicity analysis at 24, 48, and 72 h was conducted following exposure of larvae to COE. This assessment aimed to determine the lethal concentration (LC_{50}) of COE. The COE exhibited a sigmoidal dose-response curve within the tested range (0–500 μg/mL). The calculated LC_{50} values were 45.86 μg/mL at 24 hpf, 44.05 μg/mL at 48 hpf, and 42.72 μg/mL at 72 hpf (Fig. S4A). Based on these results, 5, 10, and 20 μg/mL were selected for downstream experiments. These concentrations were well tolerated, with no lethality or morphological defects observed. To establish a neurotoxicity model, we exposed the embryos (3–4 hpf) to PQ at concentrations of 25, 50, and 100 μM. Hatching rates and morphological changes were monitored from 24 to 96 hpf. At 48 hpf, a transient delay in hatching was observed in the 25 μM PQ group, compared to both controls and higher concentrations. However, by 72 hpf, hatching rates normalized across all groups (Fig. S4B). Importantly, none of the PQ-treated embryos exhibited morphological abnormalities, supporting the use of these concentrations to model sublethal neurotoxicity without

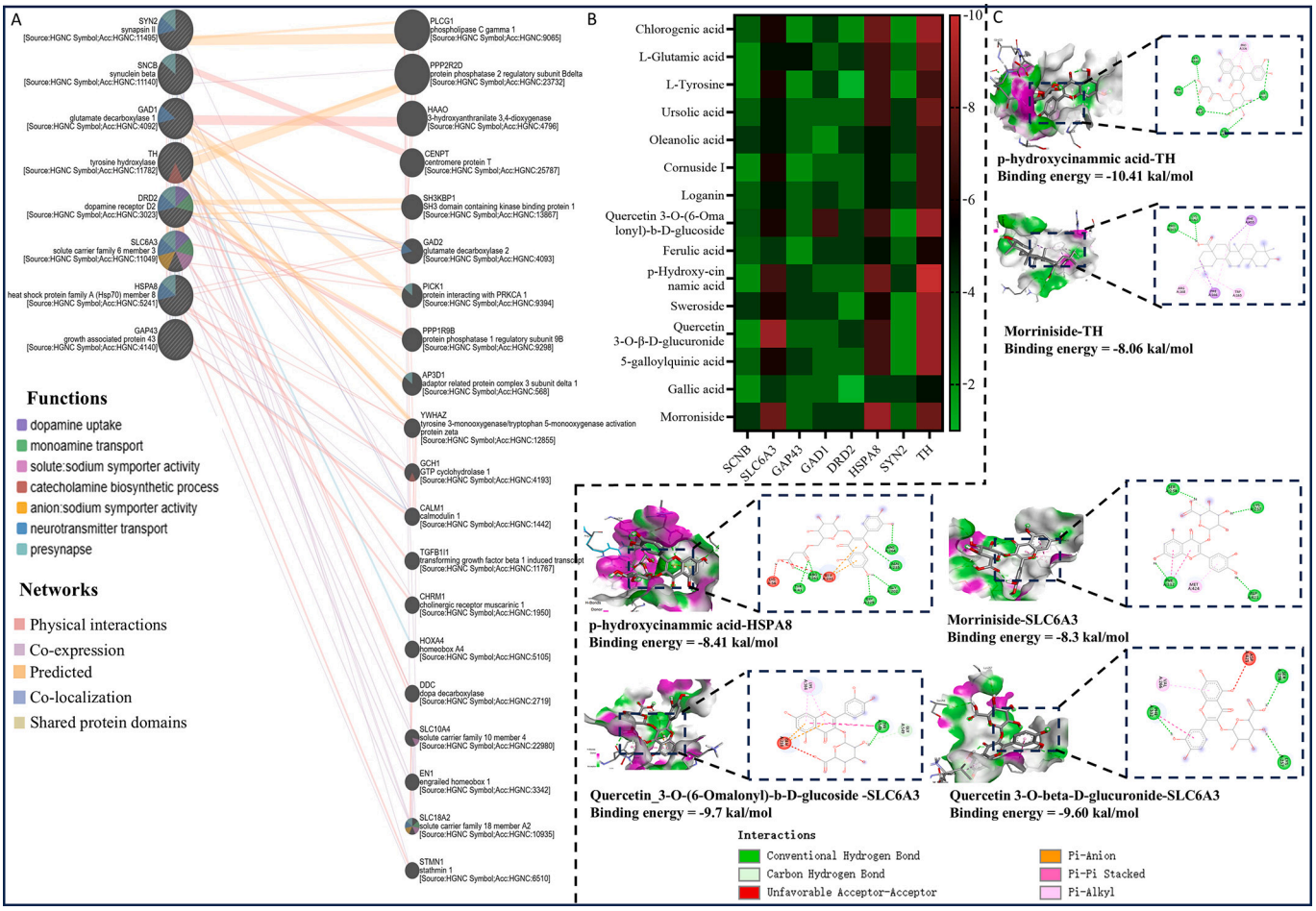

Fig. 3. Co-localization and molecular docking between COE compounds and hub genes. (A) Co-localization and functional interaction network of hub genes generated using GeneMANIA, illustrating their functional associations. (B) Heatmap showing the docking scores of COE compounds and hub genes. (C) Representative molecular docking interactions between selected COE compounds and hub genes.

inducing systemic developmental toxicity. Based on these findings and consistent with previous report (X. H. Wang et al., 2018), 100 μM PQ were selected for subsequent experiments. The combined toxicological effect of co-treatment with PQ and COE were also assessed, the percentage of hatched embryos at 48-hpf PQ-only treated group was higher compared to all other groups including controls (Fig. S4C), however, by 72 hpf the hatching normalizes in all the groups. Additionally, key morphological parameters including yolk sac area, body length, and cardiac area as indicators of physiological stress were evaluated. Across all treatment groups, none of these metrics showed significant changes (Fig. S4D-F, respectively) compared to control group, suggesting that neither individual nor combined exposure to PQ and COE impaired general embryonic development.

3.6. COE ameliorates paraquat-induced oxidative stress

PQ exert its primary toxicological effects through induction of mitochondrial oxidative stress, leading to excessive ROS production. Therefore, assessing the antioxidant potential of COE is very critical to understand its protective mechanisms. Fluorescence imaging revealed an increased ROS level in PQ-only treated larvae relative to control to group, as indicated by elevated fluorescence intensity (Fig. 4A). Co-treatment with COE (5, 10, and 20 μg/mL) attenuated ROS accumulation, with quantitative analysis confirming a dose-related reduction (Fig. 4B). Importantly, COE treatment alone at 20 μg/mL did not significantly alter basal ROS levels, possibly indicating the absence of pro-oxidant effects at this concentration. Given the reduction in ROS, we next examined the expression of antioxidant defense genes. qPCR analysis showed that PQ exposure resulted in a significant upregulation of *nrf2* compared with control embryos (Fig. 4C), consistent with a compensatory oxidative stress response. While co-treatment with COE at 20 μg/mL group showed enhanced *nrf2* expression, this increase did not reach statistical significance compared to the PQ-only group. These results suggest a potential trend where COE may support the endogenous antioxidant capacity, though further studies may be needed to confirm the activation of Nrf2–ARE signaling pathway. Notably, COE alone also demonstrate a non-significant increase in *nrf2* expression compared with control group, indicating that COE itself may support the endogenous antioxidant capacity of zebrafish larvae. In line with *nrf2* induction, *cat* expression was elevated in PQ-treated embryos (Fig. 4D), while co-treatment with 5 μg/mL COE resulted in a significant downregulation of *cat* relative to PQ alone, which may result from direct ROS-scavenging activity at this lower concentration, reducing the need for transcriptional upregulation. At 10 μg/mL, COE modestly increased *cat* expression compared with PQ alone, although this change did not reach statistical significance ($p > 0.05$). As expected, *sod2*, a key mitochondrial superoxide dismutase, was strongly upregulated following PQ exposure, reflecting persistent mitochondrial oxidative stress. COE alone induced *sod2,* this effect was also observed in *nrf2* and *cat*, further supporting its intrinsic antioxidant activity. However, co-treatment with PQ and COE did not significantly reduce *sod2* expression relative to PQ alone, except at the lowest dose, suggesting that mitochondrial superoxide production remained elevated. This persistence is consistent with PQ's well-established mechanism of redox cycling and generation of

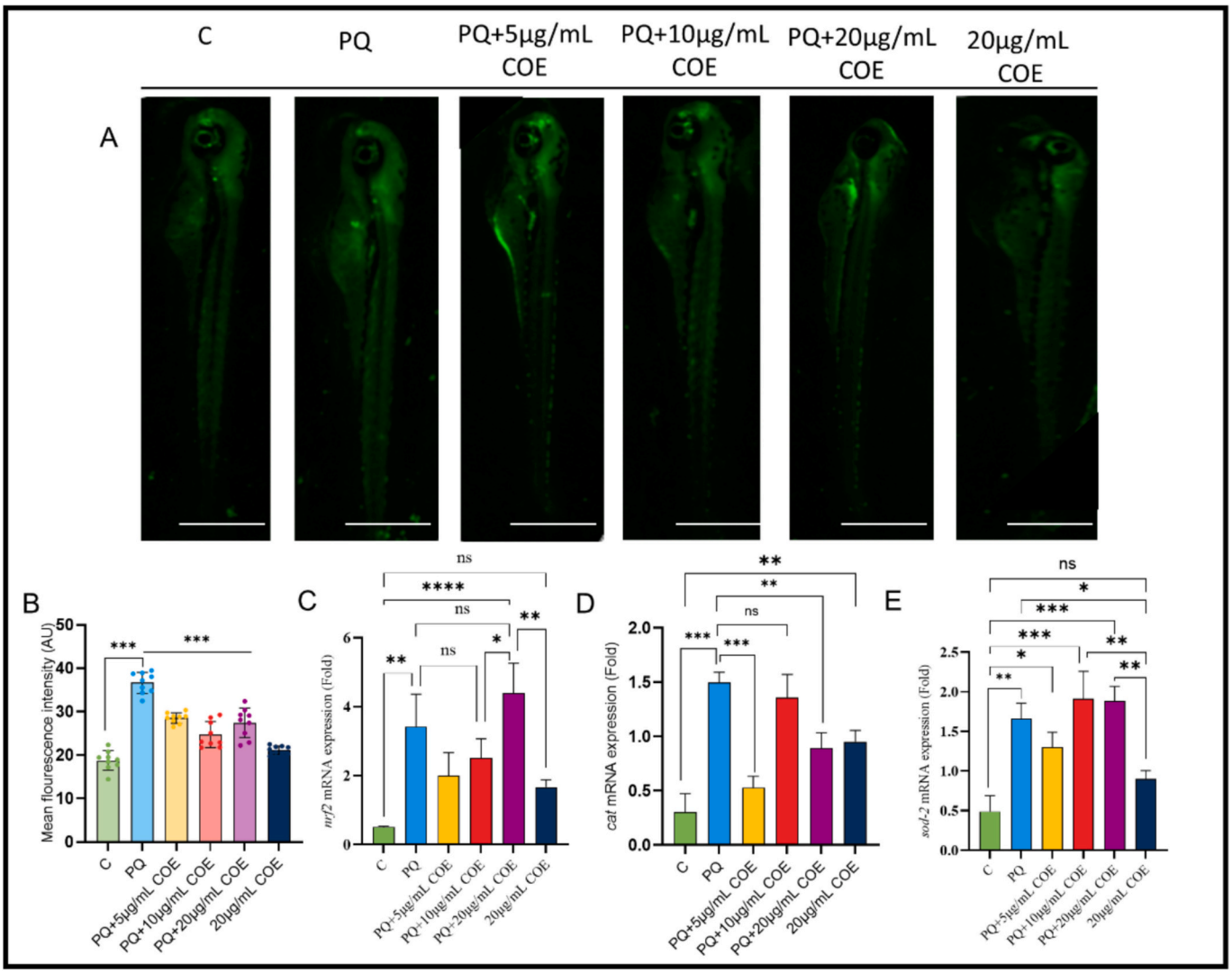

Fig. 4. Effect of COE on PQ-induced morphological changes and oxidative stress in zebrafish embryos. Representative fluorescent images of zebrafish larvae exposed to PQ or co-treated with varying concentrations of COE (A). Quantitative analysis of fluorescence intensity from larval images using ImageJ (B). C-E represent qPCR analysis of antioxidant genes: *nrf2*, *cat*, and *sod-2* mRNA expression in zebrafish larvae respectively. All data are presented as mean ± SD. Statistical significance was determined using one-way ANOVA followed by Tukey's multiple comparison test (*$p < 0.05$, **$p < 0.01$, ***$p < 0.001$; ns, not significant). Scale bars: 1.2 mm.

superoxide anions ($O_2^{\bullet-}$) within mitochondria. Sustained *sod2* induction across COE-treated groups reinforces its role as a primary line of defense against mitochondrial ROS and highlights mitochondria as a central site of PQ-induced oxidative stress (Castello et al., 2007).

3.7. COE mitigates paraquat-induced apoptosis and modulates apoptosis-related genes in zebrafish embryos

Given that excessive ROS generated by PQ may act as potent trigger of apoptotic cascades (Redza-Dutordoir and Averill-Bates, 2016), and our KEGG enrichment further support the involvement of apoptosis, we next assess whether the protective effects of COE involve modulation of apoptotic pathways. Apoptotic cell death in the larvae ware assessed using AO staining following PQ exposure or co-treatment with COE. PQ-only treated larvae demonstrated an enhanced AO fluorescence compared to control (Panel A, Fig. 5A), an indication of elevated levels of apoptosis. Notably, co-treatment with COE reduced the fluorescence intensity in a dose-dependent manner, as shown by quantitative analysis (Fig. 5B). Notably, 20 µg/mL COE exhibit the most robust anti-apoptotic effect, reducing the fluorescence close to basal levels (control levels). COE alone (20 µg/mL) did not significantly affect the apoptotic baseline, further confirming its safety at this concentration.

To gain insight into the molecular mechanisms underlying the observed protective effects, the expression of key apoptosis-regulatory genes was evaluated. Larvae in the PQ-only treated groups demonstrate a significant increase in *bcl-2* expression compared with the control group ($p < 0.01$), suggesting activation of a compensatory cellular response to counteract PQ-induced toxicity (Fig. 5A, Panel B). Co-treatment with COE (5 and 10 µg/mL) resulted in a non-significant increase in *bcl-2* expression relative to the PQ-only group, with the highest mean expression observed at 10 µg/mL. No significant difference was observed between the control group and the COE-only treated larvae. Similarly, PQ exposure significantly upregulated the pro-apoptotic gene *bax* compared with the control group (Fig. 5B). In the COE co-treated groups (5 and 20 µg/mL), *bax* expression showed a downward trend relative to the PQ-only group; however, these changes did not reach statistical significance. Notably, *bax* expression remained elevated in the 10 µg/mL COE-treated group compared with the PQ-only groups. Furthermore, *caspase-3,* a critical executioner in the apoptosis pathway was significantly elevated in PQ-treated embryos but downregulated upon COE treatment (Panel B, Fig. 5C). Moreover, COE alone did not change the basal *caspase*-3 levels as there is no statistical difference

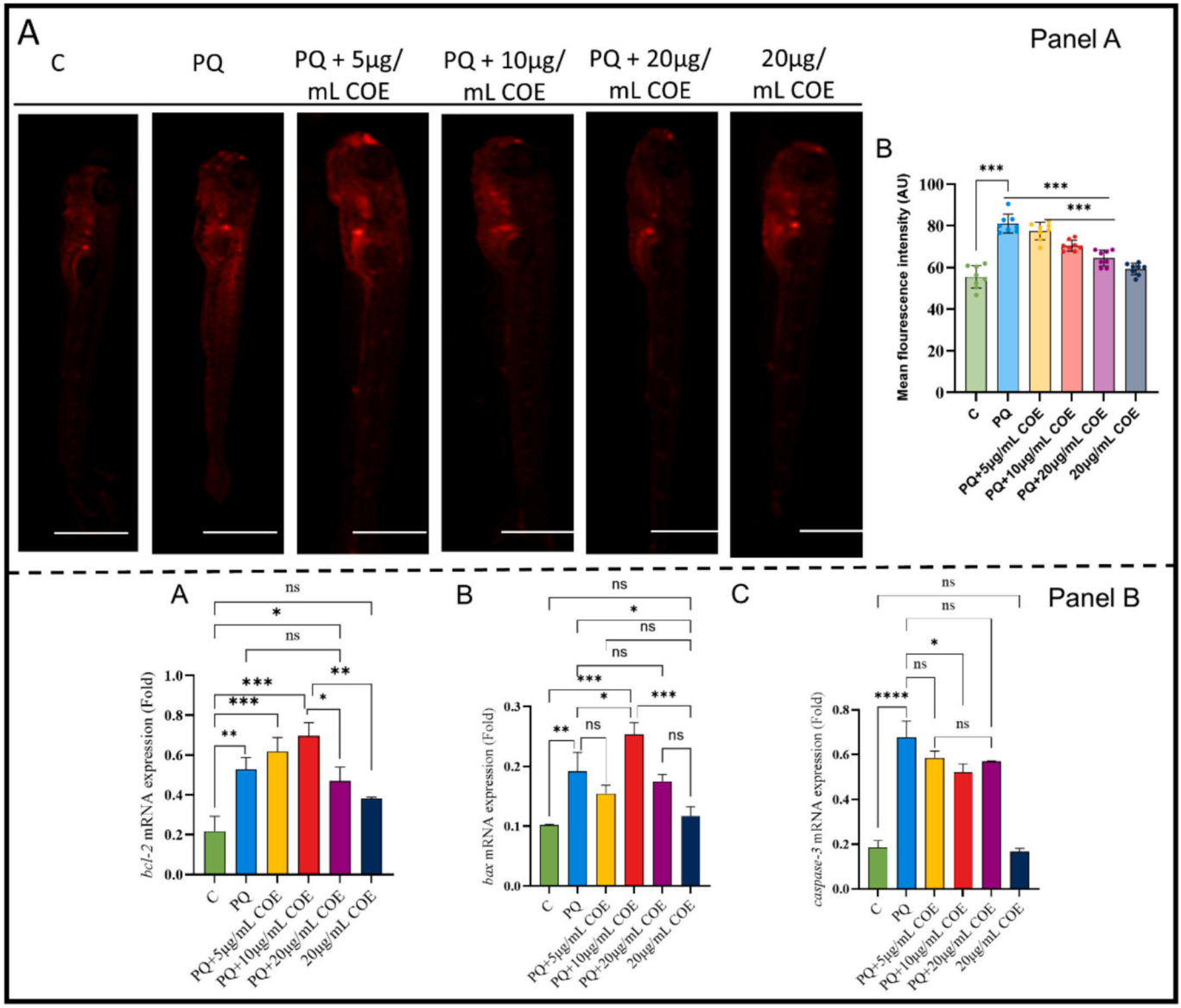

Fig. 5. Effect of COE on PQ-induced apoptosis in zebrafish embryos. Panel A: Representative fluorescence images of acridine orange (AO) staining in zebrafish larvae at 96 hpf exposed to PQ (100 µM), or co-treated with 5, 10, or 20 µg/mL of COE, or COE alone (20 µg/mL) serving as a control for extract effects (A). Quantification analysis of AO fluorescence intensity using ImageJ (B). Panel B: A-C represent relative mRNA expression of *bcl-2*, *bax*, and *caspase-3* respectively. Data are shown as mean ± SD. (*, **, *** indicate $p < 0.05$, $p < 0.01$, and $p < 0.001$, one-way ANOVA with Tukey's post hoc test) respectively. Scale bars: 1.2 mm.

between COE alone treated larvae compared with control group. This supports the AO fluorescence-based findings and indicates effective inhibition of apoptosis execution. Collectively, these data demonstrate that COE protects against PQ-induced apoptosis by modulating key apoptotic regulators, promoting anti-apoptotic signaling, and suppressing the activation of the apoptotic cascade (Panel B, Fig. 5D).

3.8. COE modulates transcriptional markers of dopaminergic signaling and synaptic vesicle dynamics in PQ-exposed zebrafish

PQ selectively impairs dopaminergic neurons, contributing to motor deficits and neurodegeneration (Rappold et al., 2011). To determine whether COE influences dopaminergic signaling as predicted from our in-silico study, we analyzed the expression of genes associated with dopamine biosynthesis (*th*), dopamine reuptake (*slc6a3*, encoding the dopamine transporter DAT), and synaptic vesicle regulation (*sncb*, *sncgb*) all which are among the hub genes. A significant downregulation of *slc6a3* and *th* was observed in PQ-only treated larvae (Fig. 6A and B, respectively), consistent with altered expression of dopaminergic markers (Gopinath et al., 2022). COE at 10 µg/mL significantly attenuated the PQ-induced alterations in both *th* and *slc6a3* expression compared with the PQ-treated group ($p < 0.05$). However, at 5 µg/mL, *slc6a3* expression was reduced relative to the PQ-only group, indicating variability in the transcriptional response across doses.

PQ-treated larvae also exhibited increased expression of *sncb* and *sncgb* (Fig. 6C and D, respectively). In contrast, co-treatment with COE resulted in a downward trend in *sncb* expression compared with PQ-only larvae, although this change was not statistically significant. Notably, *sncgb* expression was significantly reduced following COE co-treatment, suggesting that COE may influence PQ-induced dysregulation of synuclein isoforms, which have been associated with impaired synaptic vesicle trafficking and hypokinetic behavior (Milanese et al., 2012). It is worth noting that larvae treated with COE alone showed no significant changes in *th*, *slc6a3*, *sncb*, or *sncgb* expression compared with control larvae.

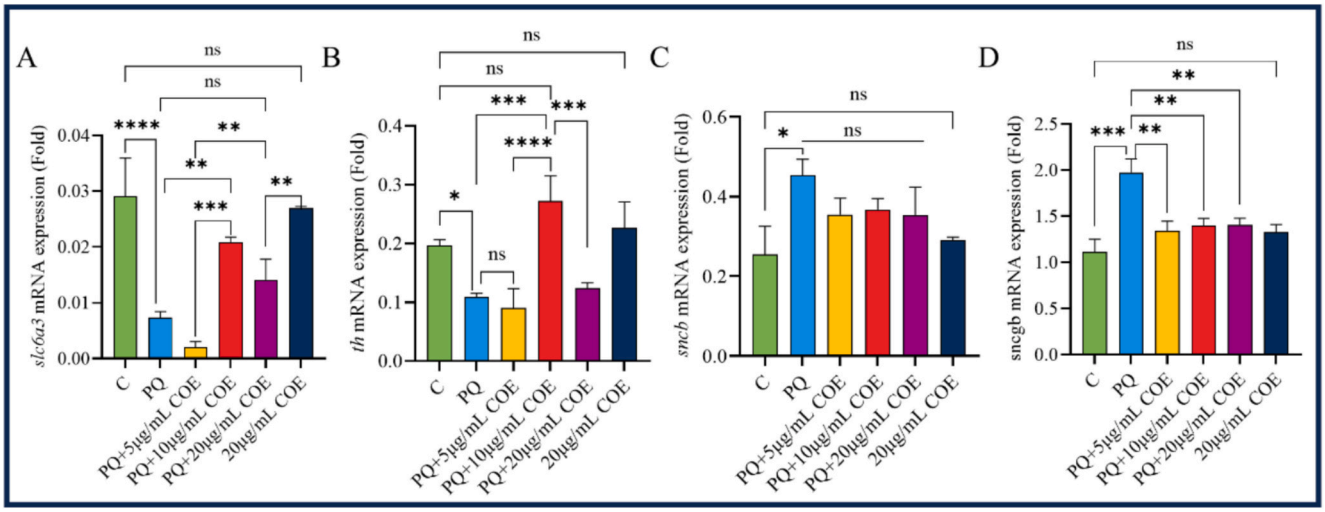

Fig. 6. Effect of COE on PQ-impaired dopaminergic system and synaptic vesicle dynamics in zebrafish embryos. Relative mRNA expression levels of dopamine transporter (DAT) (A), tyrosine hydroxylase (*th*) (B), synuclein β (*sncb*) (C), and synuclein γb (*sncgb*) (D). Data are shown as mean ± SD. (*, **, *** indicate $p < 0.05$, $p < 0.01$, and $p < 0.001$, one-way ANOVA with Tukey's post hoc test, respectively).

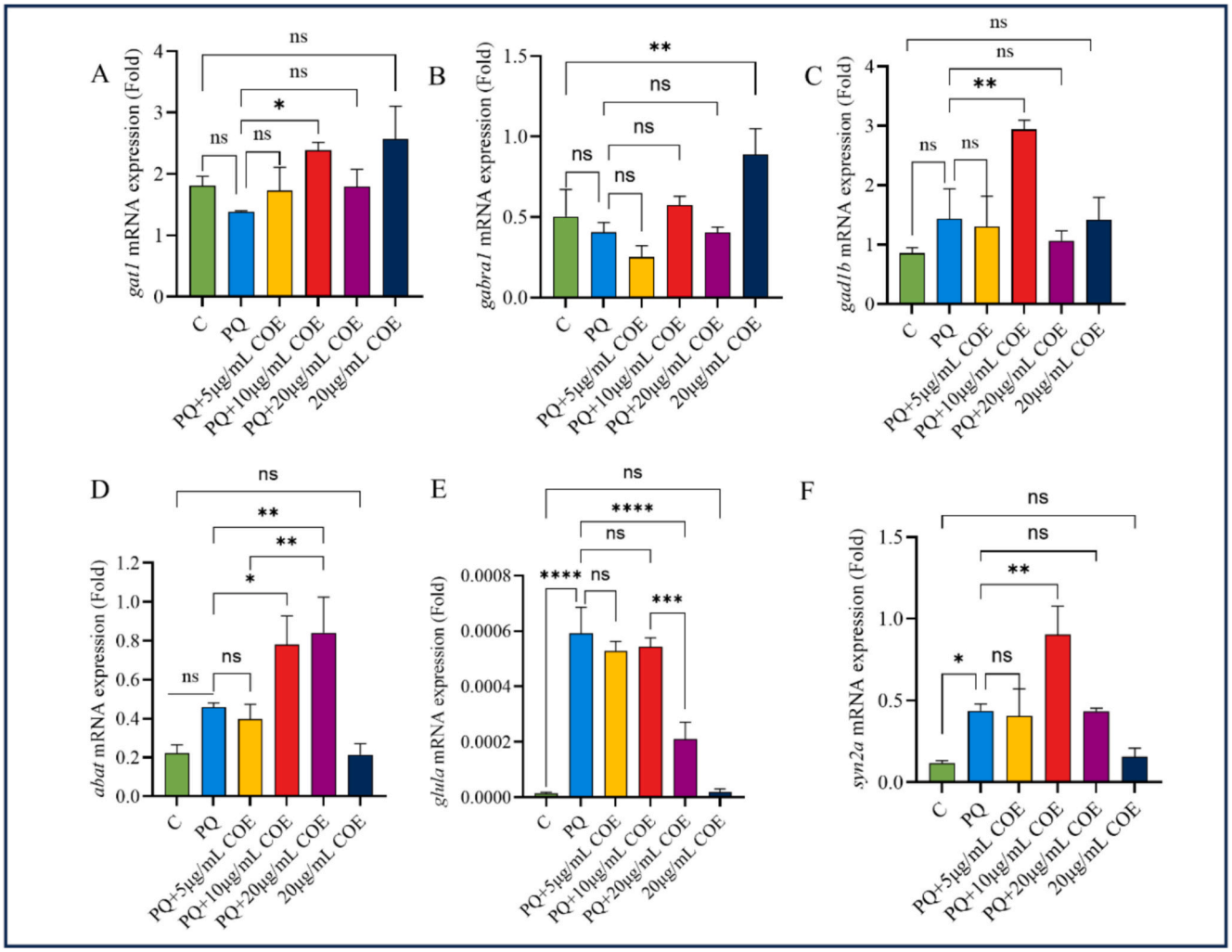

Fig. 7. Effect of COE on GABAergic neurotransmission and synaptic function in zebrafish embryos. Relative mRNA expression levels of genes involved in GABAergic (A-D) and glutamatergic (E) neurotransmission, and synaptic function (F). GABA transporter 1 (*gat1*) (A); GABA receptor alpha 1 (*gabra1*) (B); glutamate decarboxylase 1B (*gad1b*) (C); 4-aminobutyrate aminotransferase (*abat*) (D); glutaminase (*glula*) (E); and synapsin IIa (*syn2a*) (F). Data are presented as mean ± SD. Statistical significance was determined by one-way ANOVA followed by Tukey's post-hoc test. $p < 0.05$, *$p < 0.01$, **$p < 0.001$; ns, not significant.

3.9. COE modulates key components of GABAergic neurotransmission and synaptic function impaired by PQ

We hypothesized that COE may influence transcriptional markers of GABAergic and glutamatergic signaling disrupted by PQ, supported by our extensive in-silico analysis and previous evidence demonstrating that PQ perturbs neurotransmitter homeostasis and impairs neuronal excitability (Kim et al., 2022a; Lee et al., 2008). To investigate this, the expression level of key genes associated with inhibitory GABAergic transmission (*gad1b, gabra1, and abat*), excitatory glutamatergic signaling (*glula*), and synaptic function (*syn2a*) were examined. Larvae exposed to PQ-only demonstrated a decrease in *gat1* (*slc6a1*) and *gabra1* expression (Fig. 7A, and B, respectively). Although these changes did not reach statistical significance ($p > 0.05$) compared with controls. Notably, larvae co-treated with COE demonstrated an increase in expression of these genes, suggesting a possible transcriptional influence on GABA receptor and transporter regulation. Additionally, PQ-only larvae exhibit non-significant increase in *gad1b* expression compared with controls ($p > 0.05$) (Fig. 7C). COE particularly at 10 μg/mL, led to significantly higher *gad1b* expression compared with PQ alone. Consistent with this effect, COE treatment alone also stimulated *gad1b* expression, further supporting that COE likely strengthens baseline GABAergic capacity.

The expression of *abat* (GABA transaminase), a key enzyme in GABA catabolism and recycling (Besse et al., 2015), increased in PQ-exposed larvae compared with controls (Fig. 7D, $p > 0.05$). The larvae Co-treated with COE demonstrated a further significant increase in *abat* expression relative to PQ groups at 10 and 20 μg/mL. This effect is consistent with the concurrent stimulatory influence of COE (alone or in combination with PQ) on *gabra1*, *gad1b*, and *gat1*, which together possibly indicate enhanced GABA clearance. Notably, COE alone did not change basal *abat* expression compared with controls, indicating that its modulatory effect emerges primarily under PQ-induced stress conditions. PQ exposure also increased expression of glial-specific glutamine synthetase (*glula*, Fig. 7E), which likely reflects a compensatory response to excessive glutamate by promoting its conversion to glutamine. COE particularly at 20 μg/mL significantly mitigated this effect, indicating a protective effect. Similarly, PQ treated embryos demonstrate an enhanced expression of *syn2a*, associated with synaptic vesicle docking and GABA release (Fig. 7F), the observed further enhancement at COE 10 μg/mL of *syn2a* expression, likely indicate COE's role in facilitating synaptic recovery rather than merely reversing PQ-induced dysregulation considering the overall trend at this concentration. This modulation suggests that COE supports synaptic vesicle dynamics and neurotransmission under neurotoxic stress conditions.

3.10. COE promotes neuronal development and preserves neuronal structure

Consistent with the known effect of PQ to induce neuronal degeneration (Jayasinghe and Seneviratne, 2016), the expression of *gap43*, a marker of axonal growth and synaptic remodeling, significantly upregulated in PQ-only treated larvae compared with controls ($p < 0.01$; Fig. 8A), suggesting an induced transcriptional regenerative response. Interestingly, COE alone also stimulated *gap43*, and co-treatment at low and moderate doses (5 and 10 μg/mL) further potentiated the PQ-driven induction. This indicates that COE can enhance growth-associated transcriptional programs, potentially facilitating neurite extension and synaptic reorganization under stress conditions (Chung et al., 2020). By contrast, the highest COE dose (20 μg/mL) reduced *gap43* expression toward baseline (control) levels. This reversal may reflect neuroprotective effect, which diminishes the need for stress-driven regenerative response. In line with these findings, *elavl3*, a neuronal marker of differentiation and maintenance, was significantly downregulated in PQ-only treated larvae ($p < 0.01$; Fig. 8B). COE at 10 μg/mL restored *elavl3* expression. Notably, COE alone reduced *elavl3* expression relative to controls, implying that the extract likely exerts context-dependent effects: under stress, COE promotes preservation and recovery of neuronal integrity, whereas in the baseline state it may transiently alter developmental timing, leading to reduced *elavl3* transcript levels. A similar pattern was observed for Neurogenic differentiation factor 1 (*neurod1*), a redox-sensitive transcription factor required for neuronal progenitor cell maturation (Ma et al., 2022). PQ significantly suppressed *neurod1* expression relative to controls (Fig. 8C), while co-treatment with COE exhibit dose-dependent trend in *neurod1* expression level. The parallel trends of *elavl3* and *neurod1* thus suggest a coordinated action of COE in preserving neuronal identity and differentiation specifically under PQ-induced stress. Similarly, PQ exposure resulted in a significant downregulation of *mnx1* (*hb9*), a transcription factor essential for spinal motor-neuron specification and maintenance (Letchuman et al., 2022) (Fig. 8D), this effect may indicate impaired motor-neuronal maturation. Interestingly, co-treatment with COE restored *mnx1*

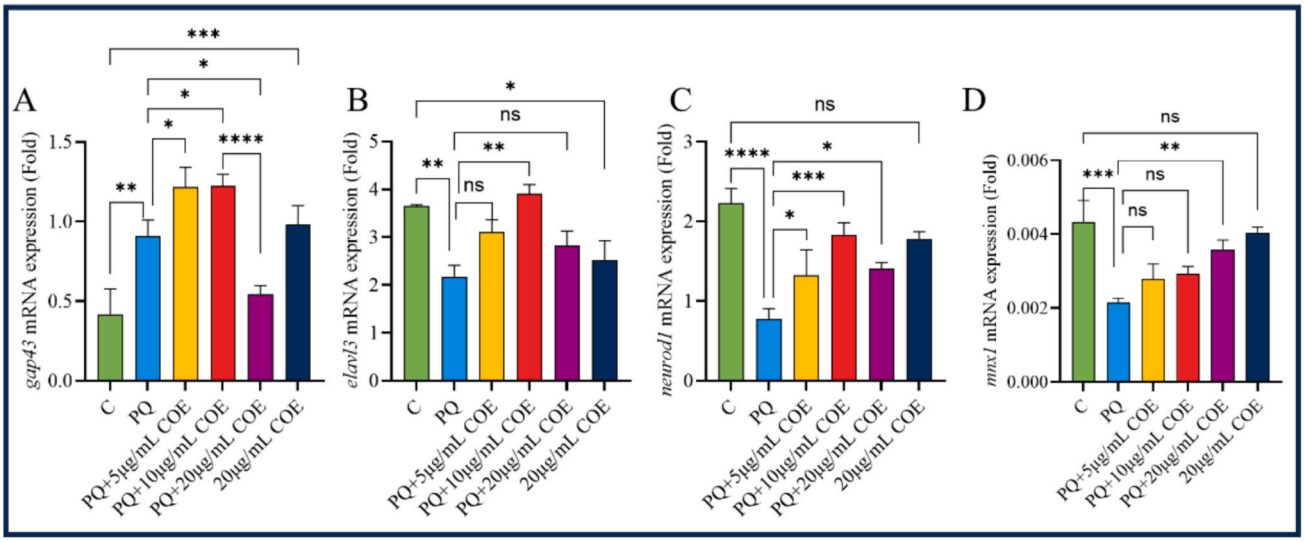

Fig. 8. Effect of COE on neuronal structure and development. Relative gene expression analysis of *gap43* (A), *elavl3* (B), *neurod1* (C), and *mnx1* (D) following zebrafish larval to PQ-exposure, co-treated with COE, or COE alone treatment. Data are presented as mean ± SD. Statistical significance was determined by one-way ANOVA followed by Tukey's post-hoc test. $p < 0.05$, *$p < 0.01$, **$p < 0.001$; ns, not significant.

expression. It should be noted that unlike *elavl3* and *neurod1*, COE alone did not affect *mnx1*, further supporting the interpretation that COE may selectively safeguards motor-neuron identity under stress induced by PQ. Collectively, these data demonstrate a coherent pattern that PQ disrupts neuronal differentiation while simultaneously triggering compensatory growth responses. COE counters these effects in a dose-dependent and context-specific manner, preserving neuronal identity and differentiation under stress.

3.11. COE preserves motor and neuronal integrity in transgenic zebrafish models

We next used transgenic zebrafish models expressing fluorescent reporters in motor neurons (Tg(Hb9:GFP)) and differentiated central neurons (Tg(HuC:GFP)) to assess the structural impact of COE on neuronal integrity (Gu et al., 2023).

In Hb9:GFP larvae, PQ induced motor axon degeneration and disorganization, evidenced by reduced fluorescence intensity and disruption of the longitudinal axonal projections in both anterior and posterior spinal regions (Fig. 9A). Quantitative analysis further confirmed a significant loss of Hb9 signal intensity in PQ-treated larvae relative to controls (Fig. 9B). Remarkably, co-treatment with COE resulted in dose-dependent protective effect, with both 10 and 20 μg/mL significantly restored fluorescence intensity. Notably, COE alone treated larvae did not show any phenotypic changes compared to control, indicating that COE effectively preserves the structural organization of motor neurons. Similarly, in HuC:GFP larvae, PQ exposure resulted in a significant reduction in HuC fluorescence, this observation is consistent with neurodevelopmental disruptions induced by PQ (Fig. 9C). Furthermore, quantitative analysis further confirmed a strong reduction in HuC signal intensity in PQ-treated larvae compared with controls (Fig. 9D). Interestingly, COE treatment demonstrated a dose-dependent trend in fluorescence intensity with 20 μg/mL restored the effect close to baseline (control levels). These data suggested that COE protects against PQ-induced neuronal injury at both the motor neuron and pan-neuronal levels. By preserving axonal structure and maintaining central neuronal

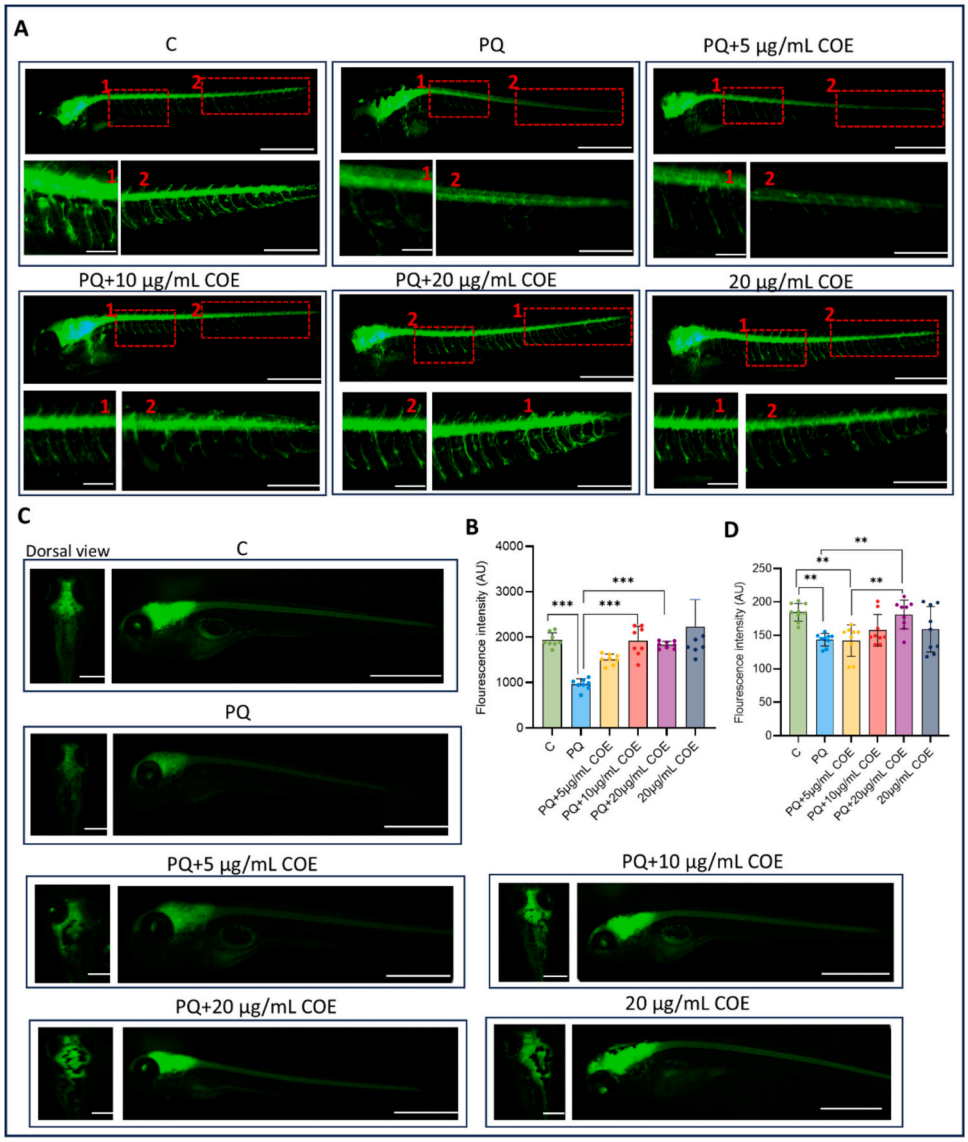

Fig. 9. COE protective effect on neuronal integrity in transgenic zebrafish embryos. A and C are representative images of transgenic Tg(Hb9:GFP) and Tg(HuC:GFP) zebrafish larvae respectively, visualizing motor neurons and differentiated neurons. Regions of interest (A) (1: anterior spinal cord; 2: posterior spinal cord) are magnified below each full-larva image. B and D, Quantification of Hb9:GFP and HuC:GFP fluorescence intensity (arbitrary units, AU) respectively, across all the treatment groups. Scale bars: full images, 1.2 mm; magnified regions, 320.1 μm. Statistical significance was determined by one-way ANOVA followed by Tukey's post-hoc test. $^{*}p < 0.05$, $^{**}p < 0.01$, $^{***}p < 0.001$.

patterning.

3.12. COE ameliorates PQ-induced behavioral deficits and improves locomotor responsiveness in zebrafish larvae

PQ is well documented to induce behavioral and neuromotor deficits in developing organisms (Ait-Bali et al., 2016). Given the structural and transcriptional neuroprotection observed with COE, we next examined whether these effects translated into improvements in larval behavior. In spontaneous locomotor activity assay, movement was tracked over a 30-min period using the Zebrabox system. PQ-treated larvae exhibited a reduced swimming activity, including decreased trajectory, shorter total distance traveled, and reduced swimming velocity compared with controls (Fig. 10A–C). These reductions may reflect neuronal dysfunction and align with our earlier findings on neuronal injury. Larvae co-treated with COE demonstrate a dose-dependent improvement, with larvae treated with 10 and 20 μg/mL COE demonstrated an improved swimming behavior (Fig. 10B) relative to PQ-only treated larvae. This effect is consistent with significant increase of swimming speeds in COE-treated groups (Fig. 10C). We next performed a light–dark transition test over a period of 30 min with alternating 5 min light and dark phases. PQ-only larvae showed less responses to light transitions, with minimal changes in locomotor activity (Fig. 10D–F), likely suggesting impaired photomotor reflexes. In contrast, COE restored light–dark responsiveness, particularly at 20 μg/mL, consistent with free locomotion assay. These observations suggest that COE not only mitigates structural neuronal damage but also preserves functional sensorimotor behaviors.

4. Discussion

PQ poisoning continues to pose a significant public health concern globally, with increasing reports across diverse populations

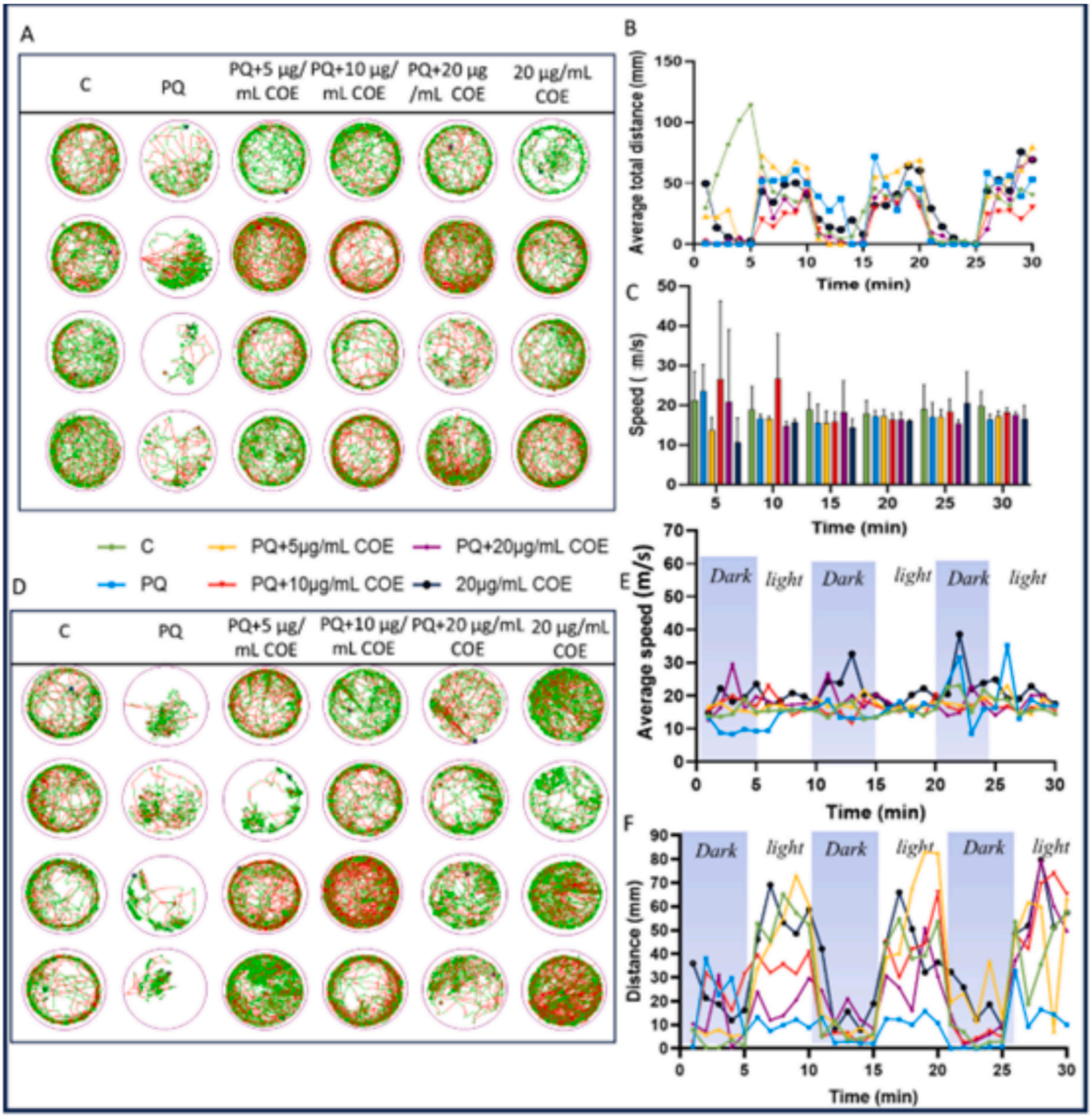

Fig. 10. Effect of COE on behavioral deficit induce by PQ in zebrafish embryos. (A) Representative swimming trajectories of zebrafish larvae expose to PQ or co-treated with COE (5, 10, or 20 μg/mL), recorded over a 30-min free-swimming period using an automated Zebrabox system using 8 dpf larvae. (B) Average total distance traveled over 30 min (C), Mean swimming speed over time. (D) Representative trajectories from the light–dark alternation test (5-min intervals). (E) Quantification of average swim speed across alternating light and dark periods. (F) Average distance traveled during light–dark cycles.

(Sabzghabaee et al., 2010; Barma et al., 2025; Chandra et al., 2021; Kanchan et al., 2015; Sriram et al., 2024). Notably, PQ exposure has been strongly associated with the onset and progression of NDs, particularly PD (Berry et al., 2010; Sharma and Mittal, 2024). Its neurotoxic effects are primarily mediated through the induction of oxidative stress and mitochondrial dysfunction (Henrich et al., 2023; Wang et al., 2018), which together disrupt cellular homeostasis. In the present study, we observed a significant upregulation of *nrf2* in PQ-treated embryos which aligns with previous findings, which indicate that the Nrf2–ARE pathway acts as a key compensatory mechanism in response to oxidative insults (Izumi et al., 2015; Wu et al., 2019). This transcriptional activation was accompanied by increased expression of downstream antioxidant genes (*sod* and *cat*), suggesting the initiation of an endogenous defense response (Nunes et al., 2017). Notably, the duration of PQ exposure appears to be critical, given its active redox cycling within mitochondria, which results in persistent generation of superoxide radicals ($O_2^{\cdot-}$). The sustained upregulation of *sod* may thus reflect an adaptive response to detoxify excessive superoxide species. This suggests that COE not only supports but induces the activation of the Nrf2–ARE pathway which has also been reported in a recent study (Fletcher, 2024).

Evidence suggest that oxidative stress is closely associated with the induction of cellular apoptosis (Redza-Dutordoir and Averill-Bates, 2016). In agreement with previous reports (Robertson and Orrenius, 2000; Nellore and Nandita, 2015; Wang et al., 2016), our findings confirm that PQ exposure elicits apoptotic responses in zebrafish embryos. Notably, the observed increase of both pro-apoptotic (*bax*) and anti-apoptotic (*bcl2*) genes compared to controls observed in PQ-treated embryos, further confirmed a compensatory response of the embryos. Similarly, it should be noted that the *bax/bcl2* ratio rather than the absolute expression levels serves as a critical determinant of apoptosis (Raisova et al., 2001). Interestingly, in COE co-treated embryos, while bax remained upregulated, the concomitant modulation of *bcl2* led to a reduced *bax/bcl2* ratio, suggesting a shift toward an anti-apoptotic state. This finding is consistent with earlier studies where iridoid glycosides from *C. officinalis* mitigated apoptosis through similar mechanisms in rodent models (Chen et al., 2016). Moreover, COE-treated embryos demonstrated only a mild modulation of *caspase-3*, a key executioner caspase in the apoptotic pathway. This attenuated response may reflect a protective effect of COE against full activation of the apoptotic machinery. A comparable trend was observed in MDA-MB-231 cells treated with COE, where *caspase-3* was modestly upregulated (Telang et al., 2019), further supporting the context-dependent anti-apoptotic role of COE.

Dopaminergic signaling is a critical regulatory axis implicated in diverse neurobiological processes, including olfactory behaviors like sniffing (Johnson et al., 2025), adolescent plasticity (Stowell and Wang, 2025), maintenance of myelin sheath integrity (Ding et al., 2020), and auditory-based social learning (Paraouty et al., 2021). Its disruption has profound implications for neurological health. PQ exposure has been well established to induce degeneration of dopaminergic neurons, thereby contributing to Parkinsonian pathology (Shimizu et al., 2003). Mechanistically, PQ promotes oxidative stress by triggering mitochondrial redox cycling, leading to excessive ROS generation, apoptosis, and related neurodegenerative cascades (See et al., 2022). Previous study reported that acute exposure (24 h) to 100 μM PQ did not alter the expression of *th* and *slc6a3* in zebrafish embryos (Wang et al., 2018). The same concentration led to a significant downregulation of *th* and *slc6a3* in the present study. However, it should be noted that, this discrepancy could be attributable to differences in duration of exposure. Supporting this, repeated intraperitoneal injections of PQ in adult zebrafish led to a reduction in *slc6a3* expression (Bortolotto et al., 2014), and chronic oral administration in mice resulted in reduced numbers of *th*-positive neurons and downregulated *slc6a3* mRNA levels in the substantia nigra (Ren et al., 2009). This molecular event induced by PQ, leads to a permanent loss of dopaminergic neurons as reported by Dwyer et al. (2021). Constant loss of this neurons is the main driver of parkinsonian disorder (Sharma and Mittal, 2024). Importantly, COE significantly mitigated the PQ-induced dopaminergic impairment, effectively restoring the expression of *slc6a3* and *th* in a dose-dependent manner. This is consistent with work by which demonstrated that morroniside, a major compound present in COE, show protective effect on dopaminergic neurons with dose-dependent trend in *th* expression in mice with MPTP-induced dopaminergic neuronal damage. Furthermore, the observed elevated expression of *sncb* and *sncgb*, which encode synaptic vesicle–associated proteins critical for vesicle trafficking, dopamine release, and synaptic plasticity (Milanese et al., 2012) in PQ-only embryos, may represent a compensatory mechanism against synaptic dysfunction or vesicle mobilization stress. However, it should also be noted that increased synuclein expression is also associated with disrupted vesicular dynamics, impaired dopamine recycling, and enhanced protein aggregation, all of which exacerbate dopaminergic cytotoxicity (Toni and Cioni, 2015). COE modestly normalized *sncb* expression and significantly reduced *sncgb* levels compared with PQ-treated larvae, while having no effect in control conditions. This suggests that COE alleviates synaptic stress by rebalancing vesicle-associated protein expression, thereby maintaining vesicle trafficking, neurotransmitter release, and dopaminergic signaling integrity. Collectively, these findings suggest that COE's neuroprotective effects may be mediated primarily through the stabilization of dopamine synthesis and reuptake pathways (via *th* and *slc6a3*) rather than direct regulation of dopamine release, with additional benefits derived from its modulation of synaptic vesicle–associated proteins (Fig. 11A).

Beyond its well-recognized dopaminergic toxicity, PQ has also been increasingly implicated in the disruption of inhibitory neurotransmission, particularly through impairment of GABAergic signaling (Kim et al., 2022b). Previous studies demonstrate that PQ contributes to excitotoxicity by elevating glutamate concentrations in the brain, leading to NMDA receptor overstimulation and excessive calcium influx, as shown in the hippocampus of prepubertal rats (Naspolini et al., 2021). Our findings reveal that PQ exposure perturbs GABAergic signaling in zebrafish, as evidenced by the reduced expression of *gad1b* and *gat1*. Such alterations are expected to compromise GABA synthesis and recycling, ultimately lowering both synaptic and extrasynaptic GABA availability. COE reversed these deficits, suggesting that COE enhances presynaptic GABA supply and reuptake, thereby stabilizing inhibitory transmission. This interpretation is reinforced by previous evidence demonstrating that iridoid glycoside-rich *C. officinalis* extracts mitigate glutamate-induced toxicity in HT22 hippocampal cells (Jeong et al., 2012). In parallel, we observed that PQ upregulated *glula* expression, indicative of increased glutamate production and a shift toward a pro-excitatory state. This observation aligns with prior reports linking PQ exposure to glutamate accumulation and excitotoxicity, partly mediated through modulation of *glula* (Naspolini et al., 2021). Conversely, COE suppressed *glula* expression in a dose-dependent manner. This down-regulation complements the GABA-supportive effects described above, suggesting that COE acts on both arms of the excitatory/inhibitory balance (Fig. 11B).

PQ has been widely implicated in the induction of cognitive, motor, and non-motor impairments (Hong et al., 2024; Zuo et al., 2023). Consistent with these reports, our study demonstrates that PQ disrupts neuronal plasticity and promotes axonal degeneration. This is reflected by alterations in the expression of *gap43*, a well-established marker of axonal growth and regeneration (Lee et al., 2023). Notably, *gap43* is predominantly expressed in excitatory neurons and its upregulation has been observed in brains following acute seizures (Nemes et al., 2017), further supporting our earlier observation that PQ induces excitotoxicity. In zebrafish groups treated with COE, particularly at low to moderate doses, *gap43* expression was further stimulated, suggesting a potential enhancement of neuronal repair. This aligns with findings from Zhao et al. (2010), who reported that intragastric administration of iridoid glycosides from *C. officinalis* elevated hippocampal *gap43* protein

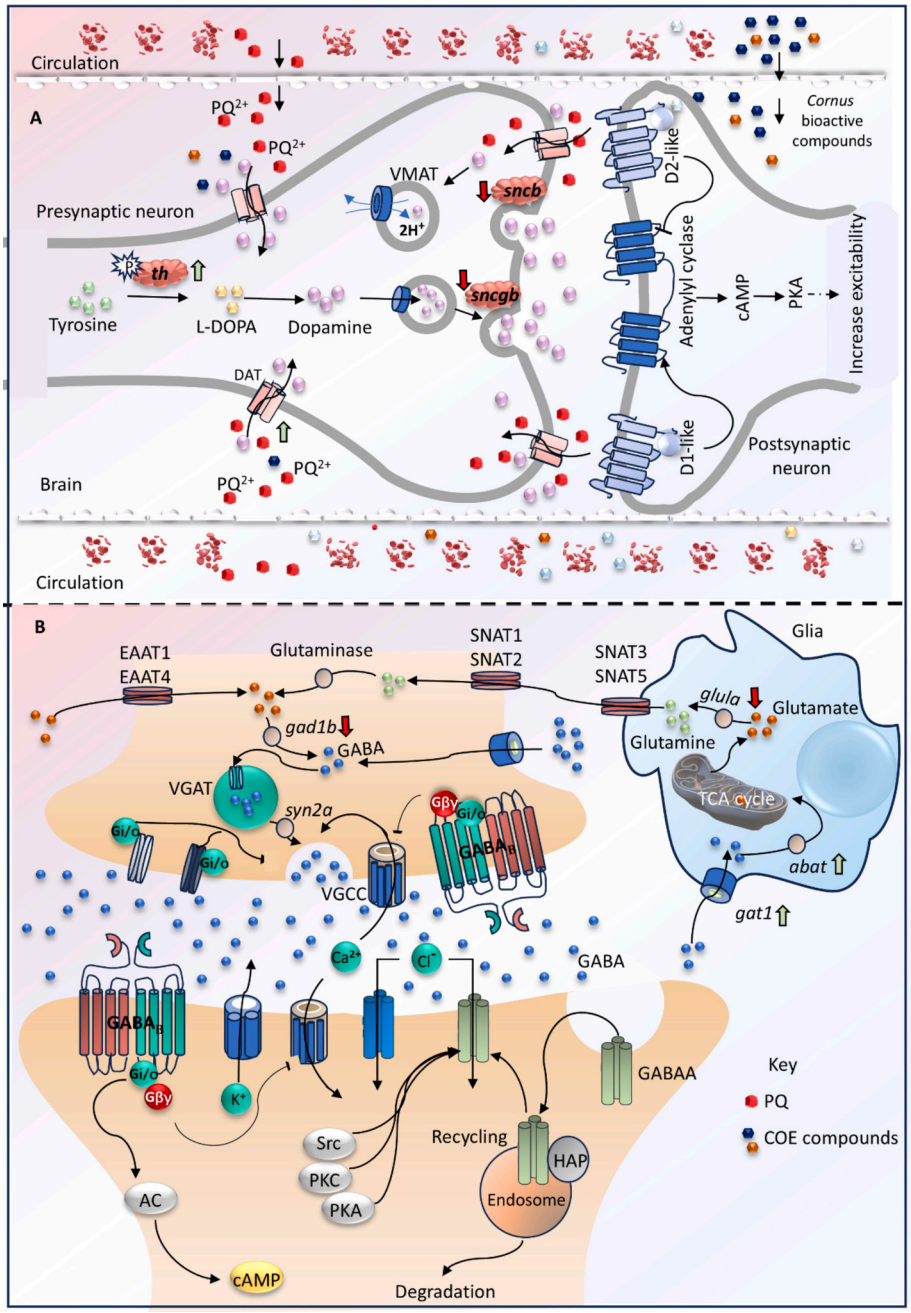

Fig. 11. Proposed mechanism of action of COE against PQ-induced toxicity. (A) Dopaminergic synapse: PQ cross blood-brain barrier and reach presynaptic dopaminergic neurons, where it disrupts dopamine synthesis, vesicular packaging, and release. PQ inhibits tyrosine hydroxylase (*th*), dopamine transporter (DAT), and disrupt *sncb* and *sncgb* which impairs synaptic vesicle dynamics. Arrows indicate sites where COE exerts protective actions to counteract PQ-induced dysfunction. (B) GABAergic synapse: PQ alters inhibitory transmission by upregulating *gad1b* expression (increasing GABA synthesis), decreasing *abat* activity (reducing GABA catabolism), and enhance *glula* (disrupting glutamate–glutamine cycling). *syn2a* dysregulation further impairs vesicle trafficking and GABA release. Arrows highlight the key sites of COE action (red arrow represent downregulation while green arrow indicate upregulation). (For interpretation of the references to colour in this figure legend, the reader is referred to the web version of this article.)

levels and improved memory in a rat brain injury model. Similarly, recent evidence indicates that loganin, a bioactive constituent of *C. officinalis*, also present in COE, alleviates MPP^+-induced neurotoxicity by upregulating *gap43* while concurrently downregulating RhoA/ROCK pathway components. These findings reinforce the notion that COE supports axonal regeneration and neuroplasticity, consistent with the stimulatory effect observed in larvae treated with 20 μg/mL COE.

Our transgenic zebrafish imaging and gene expression analyses further revealed that PQ downregulated *elavl3*, a neuronal marker whose loss is strongly associated with progressive motor deficits, cerebellar ataxia, impaired synaptic terminal formation, disrupted axonal transport, and abnormalities in neuronal polarity, as demonstrated by Ogawa et al. (2018). Similar downregulation has also been reported in zebrafish exposed to difenoconazole and isoprocarb (Wang et al., 2022; Yang et al., 2023). The remarkable restoration of *elavl3* expression observed upon COE treatment, highlight its potential to counteract PQ-induced disruption of neuronal identity and synaptic integrity. A comparable protective trend was observed with *mnx1* (hb9), a transcription factor essential for the differentiation and maintenance of motor neurons (Letchuman et al., 2022). The consistent reductions in

hb9 expression and fluorescence intensity in Tg(Hb9:GFP) larvae observed in PQ-only treated larvae, could be linked to impaired specification of cholinergic motor neurons, synaptic dysfunction, and motor impairments (Nishimaru et al., 2005; Ziskind-Conhaim et al., 2010). Thus, the restored *mnx1* expression observed here in COE co-treated larvae, suggest COE may not only mitigates toxic suppression but also reinforces the developmental transcriptional identity and resilience of motor neurons under stress.

While molecular markers capture mechanistic alterations, behavioral outcomes serve as an indispensable functional readout of neurotoxicity and therapeutic efficacy in zebrafish models (Jarema et al., 2022). In our study, PQ-exposed embryos exhibited pronounced impairments in locomotor activity, consistent with neurodegenerative phenotypes associated with dopaminergic dysfunction. These results corroborate earlier findings that PQ disrupts zebrafish motor behavior through oxidative damage and neuronal loss (Nellore and Nandita, 2015; Tantry and Santhakumar, 2024). Strikingly, COE rescued these behavioral deficits in a dose-dependent fashion, thereby underscoring its neuroprotective potential. This observation resonates with previous reports that cornuside, a major iridoid glycoside in *C. officinalis*, and also present in significant amounts in COE, ameliorates $A\beta_{1-42}$-induced cognitive impairments in mouse models (Zhou et al., 2025).

5. Conclusion

This study demonstrates that COE provides dose-dependent protection against PQ-induced neurotoxicity across molecular, cellular, and behavioral domains in zebrafish. Mechanistically, COE protect the larvae against oxidative stress, apoptosis, restores transcriptional changes in dopaminergic and GABAergic pathway genes and modestly alleviates synuclein-linked vesicular stress. Furthermore, COE promotes axonal regeneration, reinstates markers of neuronal identity and differentiation, and preserves pan-neuronal and motor-axon structure in HuC:GFP and Hb9:GFP larvae. These molecular and structural effects translate into significant functional recovery, evidenced by improved spontaneous locomotion and restored light–dark responsiveness, while gross morphological safety indices remained stable across the tested dose range. Collectively, these findings position COE as a promising candidate for mitigating pesticide-related neurotoxicity and Parkinson's disease related phenotypes. However, this study has some limitations. The findings are restricted to a zebrafish model without validation in mammalian systems and rely primarily on gene expression data without confirmation at the protein level. Moreover, only short-term effects during early development were examined, and long-term exposure outcomes remain unexplored.

CRediT authorship contribution statement

Anas Yusuf: Writing – review & editing, Writing – original draft, Visualization, Investigation, Data curation. **Murtala Bindawa Isah:** Writing – review & editing, Supervision. **Wenting Li:** Visualization, Investigation, Data curation. **Xiaozhou Yang:** Writing – review & editing. **Chen Chen:** Writing – review & editing. **Alberto C.P. Dias:** Writing – review & editing, Supervision, Conceptualization. **Xiaoying Zhang:** Writing – review & editing, Supervision, Funding acquisition, Conceptualization.

Declaration of competing interest

The authors declare that they have no known competing financial interests or personal relationships that could have appeared to influence the work reported in this paper.

Acknowledgement

This work was financially supported by the Shaanxi International Science and Technology Cooperation Base (2022GHJD-06). The Talent Initiative Project (X20240142) and the Special Project for Scientific Research and Capacity Building (X20240022) at Shaanxi University of Technology, China.

Appendix A. Supplementary data

Supplementary data to this article can be found online at https://doi.org/10.1016/j.pestbp.2026.107143.

Data availability

No data was used for the research described in the article.

References

Ait-Bali, Y., Ba-M'hamed, S., Bennis, M., 2016. Prenatal Paraquat exposure induces neurobehavioral and cognitive changes in mice offspring. Environmental Toxicology and Pharmacology 48, 53–62. https://doi.org/10.1016/j.etap.2016.10.008.

Alizadeh, S., Anani-sarab, G., Amiri, H., Hashemi, M., 2022. Paraquat induced oxidative stress, DNA damage, and cytotoxicity in lymphocytes. Heliyon 8 (7), e09895. https://doi.org/10.1016/j.heliyon.2022.e09895.

Baltazar, M.T., Dinis-Oliveira, R.J., Bastos, M. de L., Tsatsakis, A.M., Duarte, J.A., Carvalho, F., 2014. Pesticides exposure as etiological factors of Parkinson's disease and other neurodegenerative diseases—a mechanistic approach. Toxicol. Lett. 230 (2), 85–103. https://doi.org/10.1016/j.toxlet.2014.01.039.

Barma, A., Poudel, A., Rawal, G., Karn, M., Kc, U., Ojha, L., Bajgai, D., Mandal, M., 2025. Fatal paraquat poisoning: a case report and literature review on rapid deterioration and therapeutic challenges. Ann. Med. Surg. 87 (4), 2421. https://doi.org/10.1097/MS9.0000000000003103.

Bashirova, N., Poppitz, D., Klüver, N., Scholz, S., Matysik, J., Alia, A., 2023. A mechanistic understanding of the effects of polyethylene terephthalate nanoplastics in the zebrafish (*Danio rerio*) embryo. Sci. Rep. 13 (1), 1891. https://doi.org/10.1038/s41598-023-28712-y.

Berry, C., La Vecchia, C., Nicotera, P., 2010. Paraquat and Parkinson's disease. Cell Death Differ. 17 (7), 1115–1125. https://doi.org/10.1038/cdd.2009.217.

Besse, A., Wu, P., Bruni, F., Donti, T., Graham, B.H., Craigen, W.J., McFarland, R., Moretti, P., Lalani, S., Scott, K.L., Taylor, R.W., Bonnen, P.E., 2015. The GABA transaminase, ABAT, is essential for mitochondrial nucleoside metabolism. Cell Metabolism 21 (3), 417–427. https://doi.org/10.1016/j.cmet.2015.02.008.

Błaszczyk, J.W., 2016. Parkinson's disease and neurodegeneration: GABA-collapse hypothesis. Front. Neurosci. 10. https://doi.org/10.3389/fnins.2016.00269.

Bortolotto, J.W., Cognato, G.P., Christoff, R.R., Roesler, L.N., Leite, C.E., Kist, L.W., Bogo, M.R., Vianna, M.R., Bonan, C.D., 2014. Long-term exposure to paraquat alters behavioral parameters and dopamine levels in adult zebrafish (*Danio rerio*). Zebrafish 11 (2), 142–153. https://doi.org/10.1089/zeb.2013.0923.

Bukke, V.N., Archana, M., Villani, R., Romano, A.D., Wawrzyniak, A., Balawender, K., Orkisz, S., Beggiato, S., Serviddio, G., Cassano, T., 2020. The dual role of glutamatergic neurotransmission in Alzheimer's disease: from pathophysiology to pharmacotherapy. Int. J. Mol. Sci. 21 (20), 7452. https://doi.org/10.3390/ijms21207452.

Cassar, S., Adatto, I., Freeman, J.L., Gamse, J.T., Iturria, I., Lawrence, C., Muriana, A., Peterson, R.T., Van Cruchten, S., Zon, L.I., 2020. Use of Zebrafish in. Drug Discovery Toxicology. Chemical Research in Toxicology 33 (1), 95–118. https://doi.org/10.1021/acs.chemrestox.9b00335.

Castello, P.R., Drechsel, D.A., Patel, M., 2007. Mitochondria are a major source of paraquat-induced reactive oxygen species production in the brain. J. Biol. Chem. 282 (19), 14186–14193. https://doi.org/10.1074/jbc.M700827200.

Chandra, A., Shah, K.A., Mahato, S., Bhattacharjee, M.S., Mandal, T., 2021. Paraquat poisoning. BMJ Case Rep. 14 (11), e246585. https://doi.org/10.1136/bcr-2021-246585.

Chen, C., Ai, Q., Shi, A., Wang, N., Wang, L., Wei, Y., 2023. Oleanolic acid and ursolic acid: Therapeutic potential in neurodegenerative diseases, neuropsychiatric diseases and other brain disorders. Nutritional Neuroscience 26 (5), 414–428. https://doi.org/10.1080/1028415X.2022.2051957.

Chen, Y., Wu, Y., Gan, X., Liu, K., Lv, X., Shen, H., Dai, G., Xu, H., 2016. Iridoid glycoside from *Cornus officinalis* ameliorated diabetes mellitus-induced testicular damage in male rats: involvement of suppression of the AGEs/RAGE/p38 MAPK signaling pathway. J. Ethnopharmacol. 194, 850–860. https://doi.org/10.1016/j.jep.2016.10.079.

Chin, C.-H., Chen, S.-H., Wu, H.-H., Ho, C.-W., Ko, M.-T., Lin, C.-Y., 2014. CytoHubba: identifying hub objects and sub-networks from complex interactome. BMC Syst. Biol. 8 Suppl 4 (Suppl. 4), S11. https://doi.org/10.1186/1752-0509-8-S4-S11.

Chung See, W.Z., Naidu, R., Tang, K.S., 2024. Paraquat and Parkinson's disease: the molecular crosstalk of upstream signal transduction pathways leading to apoptosis. Curr. Neuropharmacol. 22 (1), 140–151. https://doi.org/10.2174/1570159X21666230126161524.

Chung, D., Shum, A., Caraveo, G., 2020. GAP-43 and BASP1 in Axon Regeneration: Implications for the Treatment of Neurodegenerative Diseases. Frontiers in Cell and Developmental Biology 8, 567537. https://doi.org/10.3389/fcell.2020.567537.

Correia de Sousa, M., Gjorgjieva, M., Dolicka, D., Sobolewski, C., Foti, M., 2019. Deciphering miRNAs action through miRNA editing. Int. J. Mol. Sci. 20 (24), 6249. https://doi.org/10.3390/ijms20246249.

Darweesh, S.K.L., Vermeulen, R.C.H., Bloem, B.R., 2024. Paraquat and Parkinson's disease: has the burden of proof shifted? Int. J. Epidemiol. 53 (5). https://doi.org/10.1093/ije/dyae126.

Davis, S.E., Cirincione, A.B., Jimenez-Torres, A.C., Zhu, J., 2023a. The impact of neurotransmitters on the neurobiology of neurodegenerative diseases. Int. J. Mol. Sci. 24 (20), 15340. https://doi.org/10.3390/ijms242015340.

Davis, A.P., Wiegers, T.C., Johnson, R.J., Sciaky, D., Wiegers, J., Mattingly, C.J., 2023b. Comparative toxicogenomics database (CTD): update 2023. Nucleic Acids Res. 51 (D1), D1257–D1262. https://doi.org/10.1093/nar/gkac833.

Ding, S., Gu, Y., Cai, Y., Cai, M., Yang, T., Bao, S., Shen, W., Ni, X., Chen, G., Xing, L., 2020. Integrative systems and functional analyses reveal a role of dopaminergic signaling in myelin pathogenesis. J. Transl. Med. 18 (1), 109. https://doi.org/10.1186/s12967-020-02276-1.

Dwyer, Z., Rudyk, C., Farmer, K., Beauchamp, S., Shail, P., Derksen, A., Fortin, T., Ventura, K., Torres, C., Ayoub, K., Hayley, S., 2021. Characterizing the protracted neurobiological and neuroanatomical effects of paraquat in a murine model of Parkinson's disease. Neurobiol. Aging 100, 11–21. https://doi.org/10.1016/j.neurobiolaging.2020.11.013.

Fan, S., Li, J., Zhang, X., Xu, D., Liu, X., Dias, A.C.P., Zhang, X., Chen, C., 2022. A study on the identification, quantification, and biological activity of compounds from *Cornus officinalis* before and after in vitro gastrointestinal digestion and simulated colonic fermentation. J. Funct. Foods 98, 105272. https://doi.org/10.1016/j.jff.2022.105272.

Fletcher, J., 2024. *Cornus officinalis* Extract Activates the Keap1/Nrf2 Pathway and Delays T1D Onset in the NOD Mouse. USF Tampa Graduate Theses and Dissertations. https://digitalcommons.usf.edu/etd/10508.

Flores-Gutierrez, C.A., Torres-Sanchez, E.D., Reyes-Uribe, E., Torres-Jasso, J.H., Reyna-Villela, M.Z., Rojas-Bravo, D., Salazar-Flores, J., 2023. The association between pesticide exposure and the development of Fronto-temporal dementia-cum-dissociative disorders: a review. Brain Sci. 13 (8), 1194. https://doi.org/10.3390/brainsci13081194.

Franz, Max, Rodriguez, Harold, Lopes, Christian, Zuberi, Khalid, Montojo, Jason, Bader, Gary D., Morris, Quaid, 2018. GeneMANIA update 2018. Nucleic Acids Res. 46 (W1). https://doi.org/10.1093/nar/gky311.

Gao, X., Liu, Y., An, Z., Ni, J., 2021. Active components and pharmacological effects of *Cornus officinalis*: literature review. Front. Pharmacol. 12. https://doi.org/10.3389/fphar.2021.633447.

Ghasemi, S.Z., Beigoli, S., Memarzia, A., Behrouz, S., Gholamnezhad, Z., Darroudi, M., Amin, F., 2023. Paraquat-induced systemic inflammation and oxidative stress in rats improved by *Curcuma longa* ethanolic extract, curcumin and a PPAR agonist. Toxicon 227, 107090. https://doi.org/10.1016/j.toxicon.2023.107090.

Gopinath, A., Mackie, P., Hashimi, B., Buchanan, A.M., Smith, A.R., Bouchard, R., Shaw, G., Badov, M., Saadatpour, L., Gittis, A., Ramirez-Zamora, A., Okun, M.S., Streit, W.J., Hashemi, P., Khoshbouei, H., 2022. DAT and TH expression marks human Parkinson's disease in peripheral immune cells. Npj Parkinson's Disease 8 (1), 72. https://doi.org/10.1038/s41531-022-00333-8.

Gu, J., Guo, L., Zhu, Y., Qian, L., Shi, L., Zhang, H., Ji, G., 2023. Neurodevelopmental Toxicity of Emamectin Benzoate to the Early Life Stage of Zebrafish Larvae (Danio rerio). International Journal of Molecular Sciences 24 (4), 3757. https://doi.org/10.3390/ijms24043757.

Guo, N., Wang, X., Xu, M., Bai, J., Yu, H., Le, Zhang., 2024. PI3K/AKT signaling pathway: Molecular mechanisms and therapeutic potential in depression. Pharmacological Research 206, 107300. https://doi.org/10.1016/j.phrs.2024.107300.

Guo, R., Xue, F., Zhang, J., Li, J., Li, H., Qiao, B., 2025. Cornel iridoid glycosides exerted neuroprotective effects against cerebral ischemia/reperfusion injury in rats via inhibiting TLR4/MyD88/NF-κB pathway. European Journal of Pharmacology 1001, 177742. https://doi.org/10.1016/j.ejphar.2025.177742.

Henrich, M.T., Oertel, W.H., Surmeier, D.J., Geibl, F.F., 2023. Mitochondrial dysfunction in Parkinson's disease – a key disease hallmark with therapeutic potential. Mol. Neurodegener. 18 (1), 83. https://doi.org/10.1186/s13024-023-00676-7.

Hong, Huihui, Li, Jingdian, Tong, Tong, Yang, Ting, Wang, Hui, Xu, Yudong, Lin, Xiqin, Lin, Jinxian, Liu, Sicheng, Luo, Kun, Yu, Zhengping, Yuan, Wei, Pi, Huifeng, Zhou, Zhou, 2024. Paraquat disrupts KIF5A-mediated axonal mitochondrial transport in midbrain neurons and its antagonism by melatonin. Sci. Total Environ., 934 https://doi.org/10.1016/j.scitotenv.2024.173119.

Izumi, Y., Yamamoto, N., Yamamoto, T., Takada-Takatori, Y., Akaike, A., Kume, T., 2015. Compensatory role of the Nrf2–ARE pathway against paraquat toxicity: relevance of 26S proteasome activity. J. Pharmacol. Sci. 129 (3), 150–159. https://doi.org/10.1016/j.jphs.2015.09.003.

Jarema, K.A., Hunter, D.L., Hill, B.N., Olin, J.K., Britton, K.N., Waalkes, M.R., Padilla, S., 2022. Developmental neurotoxicity and behavioral screening in larval Zebrafish with a comparison to other published results. Toxics 10 (5). https://doi.org/10.3390/toxics10050256. Article 5.

Jayasinghe, S.S., Seneviratne, S.A., 2016. Neurotoxic effects of paraquat. Galle Medical Journal 21 (2), 21. https://doi.org/10.4038/gmj.v21i2.7954.

Jeong, E.J., Kim, T.B., Yang, H., Kang, S.Y., Kim, S.Y., Sung, S.H., Kim, Y.C., 2012. Neuroprotective iridoid glycosides from *Cornus officinalis* fruits against glutamate-induced toxicity in HT22 hippocampal cells. Phytomedicine 19 (3–4), 317–321. https://doi.org/10.1016/j.phymed.2011.08.068.

Jiang, Y., Su, Z., Zheng, J., Hsu, C.-H., Chen, Y., 2025. Small fish making a big difference: Beloved star of environmental toxicology research in the current era. Journal of Zhejiang University. Science. B 26 (7), 613. https://doi.org/10.1631/jzus.B2500166.

Johnson, N.L., Cotelo-Larrea, A., Stetzik, L.A., Akkaya, U.M., Zhang, Z., Gadziola, M.A., Varga, A.G., Ma, M., Wesson, D.W., 2025. Dopaminergic signaling to ventral striatum neurons initiates sniffing behavior. Nat. Commun. 16 (1), 336. https://doi.org/10.1038/s41467-024-55644-6.

Kamath, T., Abdulraouf, A., Burris, S.J., Langlieb, J., Gazestani, V., Nadaf, N.M., Balderrama, K., Vanderburg, C., Macosko, E.Z., 2022. Single-cell genomic profiling of human dopamine neurons identifies a population that selectively degenerates in Parkinson's disease. Nat. Neurosci. 25 (5), 588–595. https://doi.org/10.1038/s41593-022-01061-1.

Kanchan, T., Bakkannavar, S.M., Acharya, P.R., 2015. Paraquat poisoning: analysis of an uncommon cause of fatal poisoning from Manipal, South India. Toxicol. Int. 22 (1), 30–34. https://doi.org/10.4103/0971-6580.172253.

Kim, S.S., Hwang, K.-S., Kan, H., Yang, J.Y., Son, Y., Shin, D.-S., Lee, B.H., Chae, C.H., Bae, M.A., 2022. Neurotoxicological profiling of paraquat in Zebrafish model. Neurochem. Res. 47 (8), 2294–2306. https://doi.org/10.1007/s11064-022-03615-y.

Lee, C.-Y., Lee, C.-H., Shih, C.-C., Liou, H.-H., 2008. Paraquat inhibits postsynaptic AMPA receptors on dopaminergic neurons in the substantia nigra pars compacta. Biochem. Pharmacol. 76 (9), 1155–1164. https://doi.org/10.1016/j.bcp.2008.08.006.

Lee, Y.J., Jeong, Y.J., Kang, E.J., Kang, B.S., Lee, S.H., Kim, Y.J., Kang, S.S., Suh, S.W., Ahn, E.H., 2023. GAP-43 closely interacts with BDNF in hippocampal neurons and is associated with Alzheimer's disease progression. Front. Mol. Neurosci. 16, 1150399. https://doi.org/10.3389/fnmol.2023.1150399.

Letchuman, S., Tucker, A., Miranda, D., Adkins, R.L., Aceves, M., Dietz, V., Jagrit, V., Leonards, A., Lee, Y. Il, Dulin, J.N., 2022. Transcription factor Hb9 is expressed in glial cell lineages in the developing mouse spinal cord. eNeuro 9 (6). https://doi.org/10.1523/ENEURO.0214-22.2022. ENEURO.0214-22.2022.

Li, M., Zhang, J., Jiang, L., Wang, W., Feng, X., Liu, M., Yang, D., 2023. Neuroprotective effects of morroniside from Cornus officinalis sieb. Et zucc against Parkinson's disease via inhibiting oxidative stress and ferroptosis. BMC Complementary Medicine and Therapies 23, 218. https://doi.org/10.1186/s12906-023-03967-0.

Liu, T., Zheng, F., Liu, L., Zhou, H., Shen, T., Li, Y., Zhang, W., 2024. Paraquat disrupts the blood-brain barrier by increasing IL-6 expression and oxidative stress through the activation of PI3K/AKT signaling pathway. Open Med. (Warsaw, Poland) 19 (1), 20241020. https://doi.org/10.1515/med-2024-1020.

Ma, N.-X., Puls, B., Chen, G., 2022. Transcriptomic analyses of NeuroD1-mediated astrocyte-to-neuron conversion. Dev. Neurobiol. 82 (5), 375–391. https://doi.org/10.1002/dneu.22882.

Madeira, C., Vargas-Lopes, C., Brandão, C.O., Reis, T., Laks, J., Panizzutti, R., Ferreira, S. T., 2018. Elevated glutamate and glutamine levels in the cerebrospinal fluid of patients with probable Alzheimer's disease and depression. Front. Psychol. 9, 561. https://doi.org/10.3389/fpsyt.2018.00561.

Milanese, C., Sager, J.J., Bai, Q., Farrell, T.C., Cannon, J.R., Greenamyre, J.T., Burton, E. A., 2012. Hypokinesia and reduced dopamine levels in zebrafish lacking β- and γ1-synucleins. J. Biol. Chem. 287 (5), 2971–2983. https://doi.org/10.1074/jbc.M111.308312.

Mironova, Y.S., Zhukova, I.A., Zhukova, N.G., Alifirova, V.M., Izhboldina, O.P., Latypova, A.V., 2018. Parkinson's disease and glutamate excitotoxicity. Zh. Nevrol. Psikhiatr. Im. S.S. Korsakova 118 (6. Vyp. 2), 50–54. https://doi.org/10.17116/jnevro201811806250.

Naspolini, N.F., Rieg, C.E.H., Cenci, V.H., Cattani, D., Zamoner, Ariane, 2021. Paraquat induces redox imbalance and disrupts glutamate and energy metabolism in the hippocampus of prepubertal rats. NeuroToxicology 85, 121–132. https://doi.org/10.1016/j.neuro.2021.05.010.

Nellore, J., Nandita, 2015. Paraquat exposure induces behavioral deficits in larval zebrafish during the window of dopamine neurogenesis. Toxicol. Rep. 2, 950–956. https://doi.org/10.1016/j.toxrep.2015.06.007.

Nemes, A.D., Ayasoufi, K., Ying, Z., Zhou, Q.-G., Suh, H., Najm, I.M., 2017. Growth associated protein 43 (GAP-43) as a novel target for the diagnosis, treatment and prevention of epileptogenesis. Sci. Rep. 7, 17702. https://doi.org/10.1038/s41598-017-17377-z.

Nishimaru, Hiroshi, Restrepo, Carlos Ernesto, Ryge, Jesper, Yanagawa, Yuchio, Kiehn, Ole, 2005. Mammalian motor neurons corelease glutamate and acetylcholine at central synapses. Proc. Natl. Acad. Sci. USA 102 (14). https://doi.org/10.1073/pnas.0501331102.

Nunes, M.E., Müller, T.E., Braga, M.M., Fontana, B.D., Quadros, V.A., Marins, A., Rodrigues, C., Menezes, C., Rosemberg, D.B., Loro, V.L., 2017. Chronic treatment with paraquat induces brain injury, changes in antioxidant defenses system, and modulates behavioral functions in zebrafish. Mol. Neurobiol. 54 (6), 3925–3934. https://doi.org/10.1007/s12035-016-9919-x.

O'Boyle, N.M., Banck, M., James, C.A., Morley, C., Vandermeersch, T., Hutchison, G.R., 2011. Open babel: an open chemical toolbox. J. Chem. 3 (1), 33. https://doi.org/10.1186/1758-2946-3-33.

Ogawa, Y., Kakumoto, K., Yoshida, T., Kuwako, K., Miyazaki, T., Yamaguchi, J., Konno, A., Hata, J., Uchiyama, Y., Hirai, H., Watanabe, M., Darnell, R.B., Okano, H., Okano, H.J., 2018. Elavl3 is essential for the maintenance of Purkinje neuron axons. Sci. Rep. 8, 2722. https://doi.org/10.1038/s41598-018-21130-5.

Otasek, D., Morris, J.H., Bouças, J., Pico, A.R., Demchak, B., 2019. Cytoscape automation: empowering workflow-based network analysis. Genome Biol. 20 (1), 185. https://doi.org/10.1186/s13059-019-1758-4.

Paraouty, N., Rizzuto, C.R., Sanes, D.H., 2021. Dopaminergic signaling supports auditory social learning. Sci. Rep. 11 (1), 13117. https://doi.org/10.1038/s41598-021-92524-1.

Raisova, M., Hossini, A.M., Eberle, J., Riebeling, C., Orfanos, C.E., Geilen, C.C., Wieder, T., Sturm, I., Daniel, P.T., 2001. The Bax/Bcl-2 ratio determines the susceptibility of human melanoma cells to CD95/Fas-mediated apoptosis. J. Invest. Dermatol. 117 (2), 333–340. https://doi.org/10.1046/j.0022-202x.2001.01409.x.

Ramamoorthi, K., Lin, Y., 2011. The contribution of GABAergic dysfunction to neurodevelopmental disorders. Trends Mol. Med. 17 (8), 452–462. https://doi.org/10.1016/j.molmed.2011.03.003.

Rappold, P.M., Cui, M., Chesser, A.S., Tibbett, J., Grima, J.C., Duan, L., Sen, N., Javitch, J.A., Tieu, K., 2011. Paraquat neurotoxicity is mediated by the dopamine transporter and organic cation transporter-3. Proc. Natl. Acad. Sci. USA 108 (51), 20766–20771. https://doi.org/10.1073/pnas.1115141108.

Redza-Dutordoir, M., Averill-Bates, D.A., 2016. Activation of apoptosis signalling pathways by reactive oxygen species. Biochim. Biophys. Acta, Mol. Cell Res. 1863 (12), 2977–2992. https://doi.org/10.1016/j.bbamcr.2016.09.012.

Ren, J., Zhao, Y., Sun, X., 2009. Toxic influence of chronic oral administration of paraquat on nigrostriatal dopaminergic neurons in C57BL/6 mice. Chin. Med. J. 122 (19), 2366–2371.

Riedel, G., Rüdrich, U., Fekete-Drimusz, N., Manns, M.P., Vondran, F.W.R., Bock, M., 2014. An extended ΔCT-method facilitating normalisation with multiple reference genes suited for quantitative RT-PCR analyses of human hepatocyte-like cells. PLoS One 9 (3), e93031. https://doi.org/10.1371/journal.pone.0093031.

Robertson, J.D., Orrenius, S., 2000. Molecular mechanisms of apoptosis induced by cytotoxic chemicals. Crit. Rev. Toxicol. 30 (5), 609–627. https://doi.org/10.1080/10408440008951122.

Sabzghabaee, A.M., Eizadi-Mood, N., Montazeri, K., Yaraghi, A., Golabi, M., 2010. Fatality in paraquat poisoning. Singapore Med. J. 51 (6). https://pubmed.ncbi.nlm.nih.gov/20658110/.

Sánchez-Alegría, K., Flores-León, M., Avila-Muñoz, E., Rodríguez-Corona, N., Arias, C., 2018. PI3K Signaling in Neurons: A Central Node for the Control of Multiple Functions. International Journal of Molecular Sciences 19 (12), 3725. https://doi.org/10.3390/ijms19123725.

Saputra, F., Kishida, M., Hu, S.-Y., 2024. Oxidative stress induced by hydrogen peroxide disrupts zebrafish visual development by altering apoptosis, antioxidant and estrogen related genes. Sci. Rep. 14 (1), 14454. https://doi.org/10.1038/s41598-024-64933-5.

See, W.Z.C., Naidu, R., Tang, K.S., 2022. Cellular and molecular events leading to paraquat-induced apoptosis: mechanistic insights into Parkinson's disease pathophysiology. Mol. Neurobiol. 59 (6), 3353–3369. https://doi.org/10.1007/s12035-022-02799-2.

Sharma, P., Mittal, P., 2024. Paraquat (herbicide) as a cause of Parkinson's disease. Parkinsonism Relat. Disord. 119. https://doi.org/10.1016/j.parkreldis.2023.105932.

Shimizu, K., Matsubara, K., Ohtaki, K., Shiono, H., 2003. Paraquat leads to dopaminergic neural vulnerability in organotypic midbrain culture. Neurosci. Res. 46 (4), 523–532. https://doi.org/10.1016/S0168-0102(03)00163-9.

Silva, N.J., Dorman, L.C., Vainchtein, I.D., Horneck, N.C., Molofsky, A.V., 2021. In situ and transcriptomic identification of microglia in synapse-rich regions of the developing zebrafish brain. Nat. Commun. 12 (1), 5916. https://doi.org/10.1038/s41467-021-26206-x.

Sriram, K., Mandala, M., Miriyala, R., Nalumaru, A.S., Rupesh, K.A., 2024. Death due to homicidal paraquat poisnong: a case report. Natl. Board Exam. J. Med. Sci. 2 (11), 1192–1198. https://doi.org/10.61770/NBEJMS.2024.v02.i11.014.

Stowell, R., Wang, K.H., 2025. Dopaminergic signaling regulates microglial surveillance and adolescent plasticity in the mouse frontal cortex. Nat. Commun. 16 (1), 7974. https://doi.org/10.1038/s41467-025-63314-4.

Tantry, M.S.A., Santhakumar, K., 2024. Unveiling the ototoxic effects of paraquat on zebrafish larva. Aquat. Toxicol. 273, 107030. https://doi.org/10.1016/j.aquatox.2024.107030.

Telang, N.T., Nair, H.B., Wong, G.Y.C., 2019. Growth inhibitory efficacy of *Cornus officinalis* in a cell culture model for triple-negative breast cancer. Oncol. Lett. 17 (6), 5261–5266. https://doi.org/10.3892/ol.2019.10182.

Thilini, R., Yongbo, S., Hae-Chul, P., Seong-Kyu, C., Seon-Heui, C., 2024. Rotenone exposure causes features of Parkinson's disease pathology linked with muscle atrophy in developing zebrafish embryo. J. Hazard. Mater. 480, 136215. https://doi.org/10.1016/j.jhazmat.2024.136215.

Tian, W., Zhao, J., Lee, J.-H., Akanda, M.R., Cho, J.-H., Kim, S.-K., Choi, Y.-J., Park, B.-Y., 2019. Neuroprotective Effects of Cornus officinalis on Stress-Induced Hippocampal Deficits in Rats and H2O2-Induced Neurotoxicity in SH-SY5Y Neuroblastoma Cells. Antioxidants 9 (1), 27. https://doi.org/10.3390/antiox9010027.

Tiklová, K., Gillberg, L., Volakakis, N., Lundén-Miguel, H., Dahl, L., Serrano, G.E., Adler, C.H., Beach, T.G., Perlmann, T., 2021. Disease duration influences gene expression in neuromelanin-positive cells from Parkinson's disease patients. Front. Mol. Neurosci. 14, 763777. https://doi.org/10.3389/fnmol.2021.763777.

Toni, M., Cioni, C., 2015. Fish synucleins: an update. Mar. Drugs 13 (11), 6665–6686. https://doi.org/10.3390/md13116665.

Trott, O., Olson, A.J., 2010. AutoDock vina: improving the speed and accuracy of docking with a new scoring function, efficient optimization and multithreading. J. Comput. Chem. 31 (2), 455–461. https://doi.org/10.1002/jcc.21334.

Wang, Q., Liu, S., Hu, D., Wang, Z., Wang, L., Wu, T., Wu, Z., Mohan, C., Peng, A., 2016. Identification of apoptosis and macrophage migration events in paraquat-induced oxidative stress using a zebrafish model. Life Sci. 157, 116–124. https://doi.org/10.1016/j.lfs.2016.06.009.

Wang, X.H., Christopher, L.S., Zhao, Y.H., Martyniuk, C.J., 2018. Paraquat affects mitochondrial bioenergetics, dopamine system expression, and locomotor activity in zebrafish (*Danio rerio*). Chemosphere 191, 106–117. https://doi.org/10.1016/j.chemosphere.2017.10.032.

Wang, S., Han, X., Yu, T., Liu, Y., Zhang, H., Mao, H., Hu, C., Xu, X., 2022. Isoprocarb causes neurotoxicity of zebrafish embryos through oxidative stress-induced apoptosis. Ecotoxicol. Environ. Saf. 242, 113870. https://doi.org/10.1016/j.ecoenv.2022.113870.

Wu, B., Li, H.-X., Lian, J., Guo, Y.-J., Tang, Y.-H., Chang, Z.-J., Hu, L.-F., Zhao, G.-J., Hong, G.-L., Lu, Z.-Q., 2019. Nrf2 overexpression protects against paraquat-induced A549 cell injury primarily by upregulating P-glycoprotein and reducing intracellular paraquat accumulation. Exp. Ther. Med. 17 (2), 1240–1247. https://doi.org/10.3892/etm.2018.7044.

Yang, Q., Deng, P., Xing, D., Liu, H., Shi, F., Hu, L., Zou, X., Nie, H., Zuo, J., Zhuang, Z., Pan, M., Chen, J., Li, G., 2023. Developmental neurotoxicity of difenoconazole in zebrafish embryos. Toxics 11 (4), 353. https://doi.org/10.3390/toxics11040353.

Zhang, X.-F., Thompson, M., Xu, Y.-H., 2016. Multifactorial theory applied to the neurotoxicity of paraquat and paraquat-induced mechanisms of developing Parkinson's disease. Lab. Investig. 96 (5), 496–507. https://doi.org/10.1038/labinvest.2015.161.

Zhang, Z., Zhang, S., Fu, P., Zhang, Z., Lin, K., Ko, J.K.-S., Yung, K.K.-L., 2019. Roles of glutamate receptors in Parkinson's disease. Int. J. Mol. Sci. 20 (18), 4391. https://doi.org/10.3390/ijms20184391.

Zhao, L., Ding, Y., Zhang, L., Li, L., 2010. Cornel iridoid glycoside improves memory ability and promotes neuronal survival in fimbria-fornix transected rats. Eur. J. Pharmacol. 647 (1–3), 68–74. https://doi.org/10.1016/j.ejphar.2010.08.016.

Zhao, L., Duan, H., Liu, Y., Wang, Y., Li, M., Li, M., 2024. Long-term exposure of zebrafish (*Danio rerio*) to Cr(VI): reproductive toxicity and neurotoxicity. Reg. Stud. Mar. Sci. 74, 103559. https://doi.org/10.1016/j.rsma.2024.103559.

Zhou, F., Lian, W., Yuan, X., Wang, Z., Xia, C., Yan, Y., Wang, W., Tong, Z., Cheng, Y., Xu, J., He, J., Zhang, W., 2025. Cornuside alleviates cognitive impairments induced by Aβ1-42 through attenuating NLRP3-mediated neurotoxicity by promoting mitophagy. Alzheimer's Res. Ther. 17 (1), 47. https://doi.org/10.1186/s13195-025-01695-w.

Ziskind-Conhaim, L., Mentis, G.Z., Wiesner, E.P., Titus, D.J., 2010. Synaptic integration of rhythmogenic neurons in the locomotor circuitry: the case of Hb9 interneurons. Ann. N. Y. Acad. Sci. 1198, 72–84. https://doi.org/10.1111/j.1749-6632.2010.05533.x.

Zuo, Z., Li, J., Zhang, B., Hang, A., Wang, Q., Xiong, G., Tang, L., Zhou, Z., Chang, X., 2023. Early-life exposure to paraquat aggravates sex-specific and progressive abnormal non-motor neurobehavior in aged mice. Toxics 11 (10), 842. https://doi.org/10.3390/toxics11100842.